Rheology of partially molten plagioclase containing wetting silica-rich anhydrous melt

Alexandre Dimanov

Geophysical Journal International

Rheology of partially molten plagioclase containing wetting silica-rich anhydrous melt
abbreviated title: Rheology of partially molten plagioclase

Journal:	*Geophysical Journal International*
Manuscript ID	GJI-21-0714.R3
Manuscript Type:	Research Paper
Date Submitted by the Author:	n/a
Complete List of Authors:	Dimanov, Alexandre; Ecole Polytechnique
Keywords:	Creep and deformation < COMPOSITION and PHYSICAL PROPERTIES, Microstructure < COMPOSITION and PHYSICAL PROPERTIES, Plasticity, diffusion, and creep < COMPOSITION and PHYSICAL PROPERTIES, Rheology: crust and lithosphere < TECTONOPHYSICS
Additional Keywords:	

Rheology of partially molten plagioclase containing wetting silica-rich anhydrous melt

abbreviated title: **Rheology of partially molten plagioclase**

Alexandre Dimanov

LMS, UMR7649, Ecole Polytechnique

Route de Saclay, 91128 Palaiseau, France.

Corresponding author: Alexandre Dimanov, *e-mail: dimanov@lms.polytechnique.fr*

Abstract

The present work explores the effects of melt chemistry on diffusion controlled creep of partially molten labradorite plagioclase (An_{50}) at anhydrous conditions. Using sol-gel and hot pressing techniques we produced: 1) nominally melt-free samples, with < 1 vol. % residual glass confined solely to multiple-grain junctions; 2) two types of partially molten samples, containing respectively ~ 1 and ~ 5 vol. % silica-rich partial melts, wetting numerous grain boundaries by thin (< 10 nm) amorphous films. Energy dispersive X-ray analysis showed that the amorphous phases of the latter materials contained ~ 85 and 95 wt. % SiO_2, thus representing different polymerization degrees. Infrared spectroscopy showed that the initial traces of water (~ 0.05 wt. %) were dried out by annealing in air above 1100°C. Uniaxial creep tests performed at temperatures and flow stresses ranging respectively between 1100 – 1250°C and 3 – 60 MPa showed dominantly linear viscous flow, with a strong grain size dependence indicating grain boundary diffusion control. Counter-intuitively strength and activation energy increased with the content of melts. However, for the sample suite silica content co-varies with melt proportion, and thus our results suggest that the kinetics of grain boundary diffusion controlled creep strongly depends on melt chemistry. Instead of acting as short–cut for diffusion, thin films of highly viscous amorphous phases may in turn considerably hinder grain boundary transport properties.

Key words: "creep and deformation", "plasticity, diffusion, and creep", "microstructure", "rheology: crust and lithosphere"

1. Introduction

The dynamics of various tectonic settings depend on the rheological properties of partially molten silicate rocks. The stability of the high plateau resulting from the collision context of the Himalayan-Tibetan orogen is proposed to be ensured by channel flow localized within the lower crust, and

characterized by exceptionally low viscosity owing to partial melting (Harris, 2007). The accretion of oceanic crust from magma chambers beneath mid-ocean ridges involves lateral flow of gabbroic magmatic suspension, as demonstrated by bedding fabrics presenting shape preferred textures, without crystal preferred orientations (Nicolas and Ildefonse, 1996; Ildefonse and Nicolas, 1997). Lamoureux et al. (1999) and Nicolas and Ildefonse (1996) proposed that magmatic flow could operate at melt fractions as low as 10 vol. %, provided grain sliding and dissolution – precipitation creep mechanisms.

Partially molten silicates rocks are usually substantially weaker than their fully crystalline counterparts (Vigneresse et al., 1996). The extent of softening depends on several different (and sometimes interdependent) physical aspects, such as: 1) the volume fraction of the molten phase and its grain scale topology, 2) the dominant creep mechanisms, 3) the mineralogy and chemistry of the considered system. Extreme softening of partially molten silicate rocks is observed in two cases. On the one hand, if the melt fraction exceeds the so called Rheologically Critical Melt Percentage (RCMP, typically > 20 vol.%), the rock experiences loss of cohesion and a switch from ductile mechanisms to enhanced granular and cataclastic type of flow (van der Molen and Paterson, 1979). On the other hand, at low melt fractions (< 10 vol.%), grain size sensitive creep may be promoted by dissolution-precipitation and diffusional mass transfer through the molten phase (Cooper and Kohlstedt, 1984; 1986; Dell'Angelo et al.,1987). The latter mechanisms are especially efficient when large proportions of grain boundaries are lost to the melt, and thus the extent of weakening strongly depends on the grain–scale melt distribution (Cooper et al., 1989; Kohlstedt, 1992; Hirth and Kohlstedt, 1995; Dimanov et al., 1998; 2000).

Melt topology depends essentially on the wetting angle θ, which is defined as the dihedral angle between the solid – liquid interfaces of two neighboring grains, at a melt-bearing triple junction. The dihedral angle θ depends on the local equilibrium of interfacial tension forces (Beere, 1975; Bulau et al., 1979; Jurewitz and Watson, 1985; Fujii et al., 1986). The limit case $\theta = 60°$ corresponds to non-wetting melt, forming isolated spherical pockets. When $60° > \theta > 0°$, the melt forms an interconnected network

of tubules along three– and higher order grain junctions. The smaller is θ, the larger is the proportion of wetted grain boundaries and the more efficient are the diffusive mass transfer processes. The limit case θ = 0° corresponds to wetting melt, spreading as melt films along all grain boundaries. For the usual mafic and felsic silicates the dihedral angles range between 10 – 40°, and therefore, silicate melts form interconnected networks along multiple grain junctions (Kohlstedt, 1992; Laporte et al., 1997). In more details however, melt topology is sensitive to mineralogy and chemistry, to grain size distribution, but also to the mechanical stress state (Fujii et al., 1986; Dell'Angelo et al., 1987; Dell'Angelo and Tullis, 1988; Bussod and Christie, 1991; Jin et al., 1994; Hirth and Kohlstedt, 1995; Laporte and Watson, 1995; Drury and FitzGerald, 1996; Wirth, 1996; Franz and Wirth, 1997; Daines and Kohlstedt, 1997; Laporte et al., 1997; Jung and Waff, 1998; Cmíral et al, 1998; Schäfer and Foley, 2002, Walte et al., 2003; Dimanov et al., 2000; De Kloe et al, 2000; Wark et al., 2003; Mecklenburgh and Rutter, 2003; Hier-Majumder et al., 2004; Katz et al., 2006; Holtzman and Kohlstedt, 2007; Spiess et al., 2012; Carapic et al., 2013).

At low melt fraction, the extent of weakening in the grain–size sensitive regime is strongly conditioned by the melt topology, because the diffusion coefficients in silicate melts are usually much faster than in the solid or along grain boundaries. Partial melts confined solely to multiple grain junctions cause only little to moderate weakening (Cooper and Kohlstedt 1984; 1986; Kohlstedt, 1992; Hirth and Kohlstedt, 1995; Dimanov et al., 1998). Conversely, melt films wetting numerous grain boundaries induce substantial creep rate enhancement (Raj, 1982; Pharr and Ashby, 1983; Cooper et al., 1989; Paterson, 2001; Dimanov et al., 2000). To date, the influence of melt chemistry on creep rates has only been considered from the view point of the dihedral angles (Wanamaker and Kohlstedt, 1991; Kohlstedt, 1992; Wolfenstine and Kohlstedt, 1994). Yet, because diffusivities differ by orders of magnitude depending on the considered species and melt composition (Zhang et al., 2010), it may be expected that the chemical composition of the molten phase may also influence the mass transfer kinetics, and hence the creep rates.

In the present work we focus on the rheological effects of melt chemistry at high silica content (> 80 wt. % SiO_2) for partially molten plagioclase aggregates presenting wetted grain boundaries.

2. Experimental procedures

2.1. Specimen preparation

We used fine grained (< 16 μm) synthetic glass powder (Corning Inc.), with $An_{50}Ab_{50}$ (labradorite) chemical composition. X – ray fluorescence (XRF, SRS 303AS) showed that the impurity content was less than 1 wt. % (Table 1). After being stored at 120°C in oven for 24 hours, the powder was first uniaxially cold – pressed at 300 MPa in steel jackets of 20 mm in length, 10 mm in diameter and 0.5 mm thick. Then, the green bodies were subjected to hot – isostatic pressing (HIP) for 3 hours at 1150°C and 300 MPa in a gas-medium Paterson apparatus, resulting in nearly glass – free polycrystalline material, with about 1 vol. % residual glass (Dimanov et al., 1998; 1999; 2000; 2003; Rybacki and Dresen, 2000). However, this procedure results sometimes in spherulites due to fast crystallization kinetics (Rybacki and Dresen, 2000). Hence, the HIPed samples were re-crushed and milled in alcohol in an agate mortar to obtain homogeneously grained crystalline powders. Laser – particle analysis (Fritsch analysette 22) showed that about 80% of the grains were < 10 μm. The larger particles constituted agglomerates of smaller grains. The chemical composition of the powder was checked by XRF (Table 1). To remove adsorbed water, the crystalline powders were annealed at 800°C for 24 hours in air and subsequently stored in an oven at 120°C prior to further processing.

Melt–free samples

Nominally melt-free samples were first produced, in order to have a rheological reference. The prepared crystalline powders were subjected to a second round of cold- and hot-pressing. HIP at 1150°C and 300 MPa for 24 hours. The resulting materials, further referred to as “Lab” samples, are dense and

polycrystalline. They are considered as nominally melt-free, although small amounts (< 1 vol. %) of residual amorphous phase persisted at multiple grain junctions.

Scanning electron microscopy (SEM, Zeiss DSM 962) and the line intercept method were applied on polished and thermally etched specimens (Dimanov et al., 1998, 1999, 2000; 2003). The obtained microstructures are characterized by lath shaped grains with aspect ratios of 2 to 3, and log – normal grain size distribution (Fig. 1a). A mean arithmetic grain size of 9.8 ± 3.2 μm was obtained from five SEM micrographs, based on the linear intercept method and a correction factor accounting for the aspect ratio (for further details, see Dimanov et al., 1998).

Transmission electron microscopy (TEM, Philips CM 200 Twin) showed that nearly half of the grains present numerous and dense growth twins, but average dislocation densities are low (< 10^7 cm^{-2}) (Fig. 2a). Residual amorphous phase with plagioclase-like composition may remain at some multiple grain junctions (Fig. 2b).

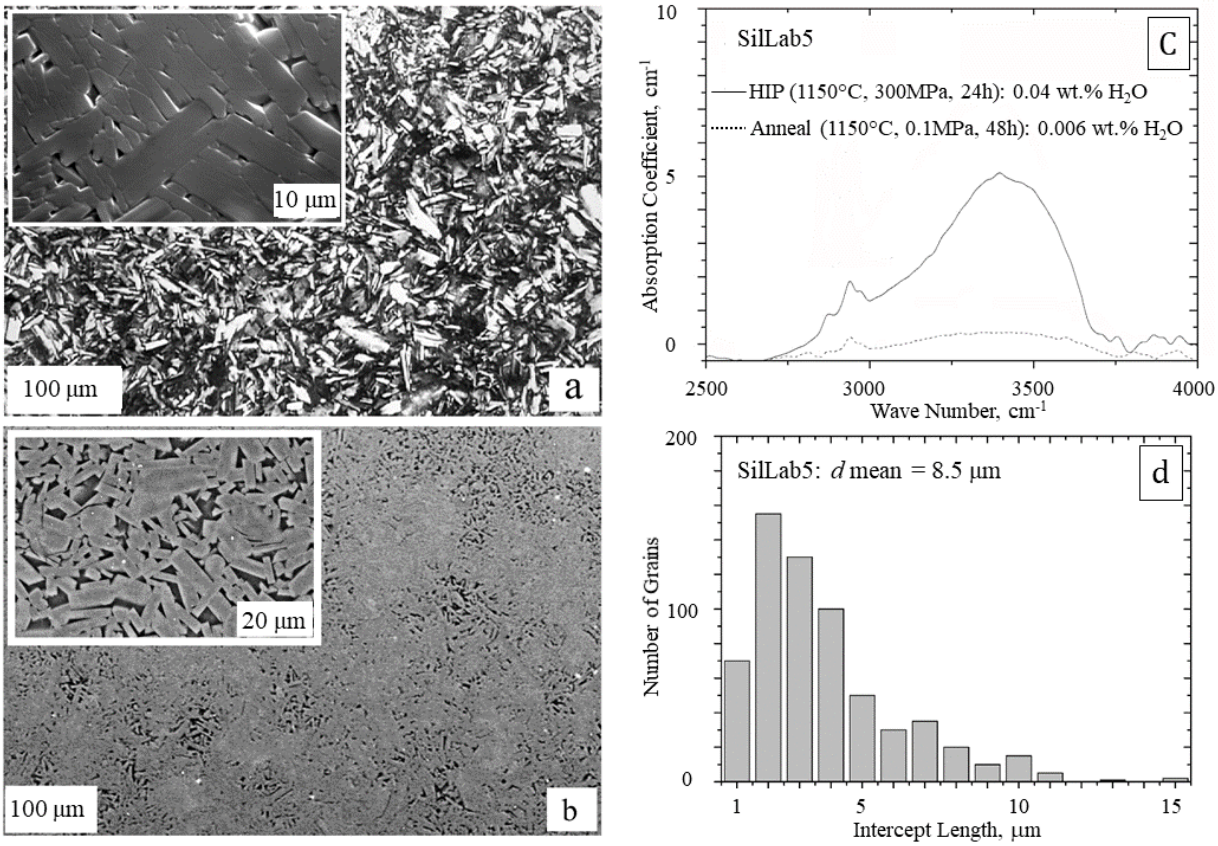

Fig. 1: Characterization of microstructures at optical and SEM scales. a) Optical micrograph of large representative area from thin section and SEM micrograph (insert, SE mode) of polished and thermally etched melt - free specimen (Lab). b) SEM micrographs (BSE mode) of polished melt-bearing specimen (SilLab5). At sub-mm scale melt distribution shows local heterogeneities, with local melt fractions reaching up to 10 vol. % (insert). c) Water content after initial HIP and after drying anneal from FTIR measurements on SilLab5 samples d) Grain size distribution for SilLab5 samples obtained by the intercept method performed on SEM micrographs.

Fluid inclusions were also observed within crystals, at grain boundaries and in the glassy-phase. Fourier transform infra-red spectroscopy (FTIR, Brüker IFS 66v) was applied on 5x5 mm^2 doubly polished sections of 150 µm in thickness. We operated in the range 2000 - 4000 cm^{-1} and we applied a third – order polynomial fit for background correction. We observed a broad absorption band centered at about 3350 cm^{-1} (Fig. 1c), indicating free molecular water present in intra – and inter – crystalline fluid inclusions, and/or dissolved within the residual glass and at grain boundaries (Dimanov et al., 1999). A few sharp peaks indicated that hydrous species were also incorporated within the crystalline structure (Hofmeister and Rossman, 1985; Beran, 1986; 1987). The samples contain 0.05 ± 0.025 wt. % H_2O (≈ 6000 ± 3000 ppm H/Si), based on the calculation approach of Paterson (1982) and the linear molar absorptivity coefficient for plagioclase (Beran, 1987). For further details, see Dimanov et al. (1998; 1999) and Rybacki and Dresen (2000). The incorporated water is due to adsorption onto the starting glass and crystalline particles, during temporary storage and handling at room condition for cold–pressing. Annealing of the samples for 24 – 48 hours in air at temperatures above 1100°C at 0.1 MPa resulted in drying out most of the water traces down to < 0.002 wt. % H_2O (Fig.1, Dimanov et al., 1999).

Table 1. Composition of starting materials and partial melts

Element	An50 glass powder*	An50 crystal powder*	Sol-gel silica*	An50 residual glass**	SilLab5 melt**	SilLab1 melt**
Na_2O(wt.%)	5.68	5.16	0.04	5.5	1.1	2.7
Al_2O_3(wt.%)	28.43	29.07	0.23	29.0	3.3	8.7
SiO_2(wt.%)	55.27	54.82	99.53	53.0	94.8	85.4

CaO(wt.%)	10.52	10.81	0.12	12.0	0.7	2.2
MgO(wt.%)	0.25	0.31	0.06	0.3	0.0	0.0
FeO(wt.%)	0.03	0.04	0.0	0.2	0.2	0.5
Cr_2O_3(wt.ppm)	0.0	0.0	0.0	0.0	0.0	0.3
ZrO_2(wt.ppm)	173	166	0.0	0.0	0.2	0.1
Total(wt.%)	100.2	100.22	98.98	100	100.3	99.9

* XRF analysis of powders, **EDX analysis in TEM

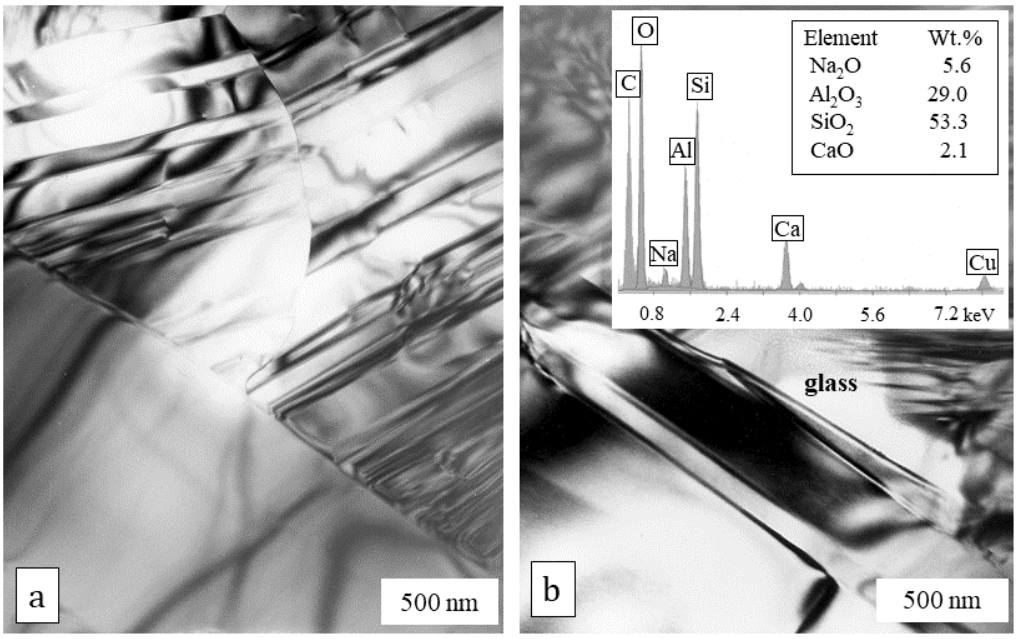

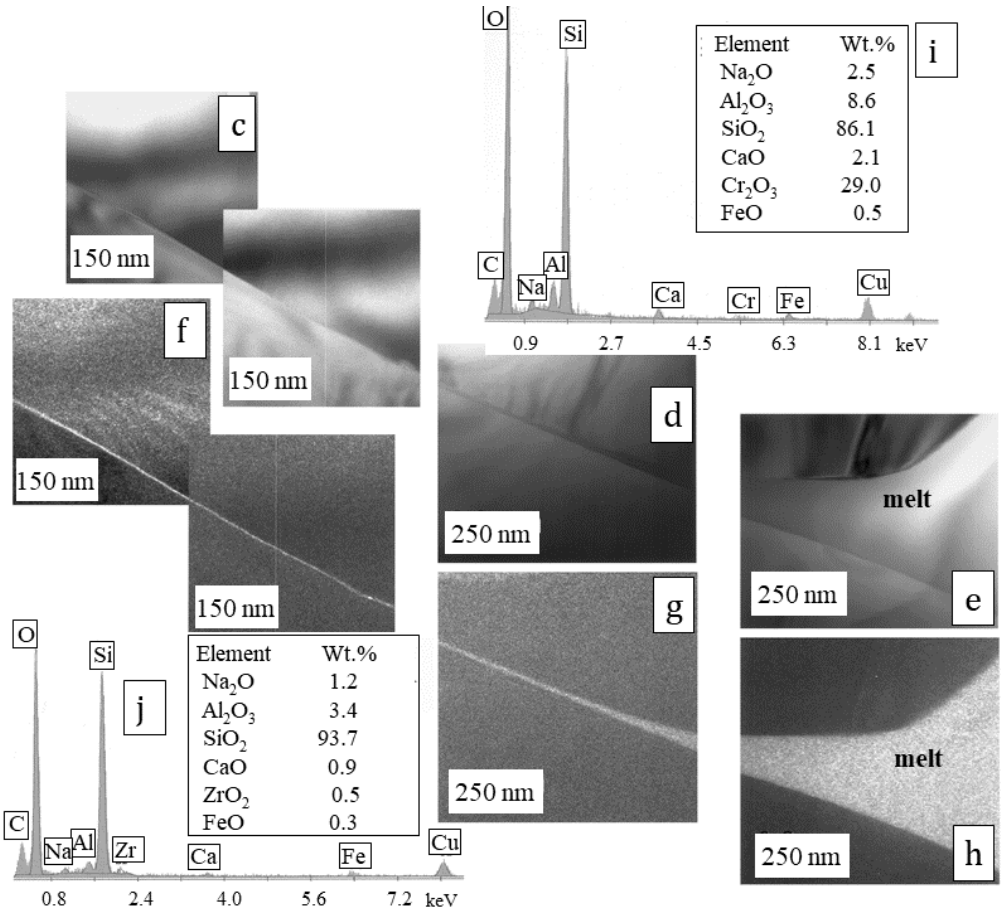

Fig. 2: Characterization of microstructures at TEM scale and EDX analysis of the chemical composition of amorphous phases. a) Grains exhibit low dislocation densities, but growth twins are numerous. b) Residual glass pockets (< 1 vol.%) are commonly found at multiple grain junctions in Lab samples. EDX analyses (insert) show that their composition is comparable to plagioclase. c-h) SilLab1 and SilLab5 materials present amorphous pockets at multiple junctions, but most interfaces also show thin amorphous films (< 10 nm) extending from triple junction channels, as evidenced by bright versus dark field imaging. i-j) EDX analysis of amorphous phases performed at melt pockets located at multiple grain junctions in SilLab1 and SilLab5 samples. Note that carbon coating of the non-conductive samples results in the presence of carbon.

Melt – bearing samples

Dimanov et al. (2000) studied partially molten labradorite materials with a few percent of melt wetting numerous grain boundaries and containing up to 80 wt. % SiO_2. These samples showed to be substantially weaker that their fully crystalline counterparts. In the present study we aimed to investigate the rheological effects of wetting melts with variable and higher silica contents. For this purpose, we

applied the sol–gel method (Hamilton and Henderson, 1968), which was previously used to precipitate synthetic basalt onto olivine crystalline powders (Cooper and Kohlstedt, 1984; Beeman and Kohlstedt, 1993; Hirth and Kohlstedt, 1995). We used pure grade tetraethyl orthosilicate ($Si(C_2H_5O)_4$, TEOS from Aldrich) diluted with ethanol in proportions of 10 to 1. Ammonium hydroxide solution (1 mol/l, Prolabo) was used as catalyst. In the solution, water hydrolyzes the TEOS and produces silanol groups (Si-OH), which interact through hydrogen bonding and form hydrolyzed silica. After drying out all volatiles, we performed XRF analysis on the precipitation product that consisted of nearly pure silica (Table 1). We prepared two aqueous solutions, where labradorite powders and diluted TEOS were mixed at the appropriate proportions in order to obtain 1 and 5 vol. % excess silica. The precipitation took place within a few minutes after the addition of the ammonium hydroxide, but the suspensions were continuously stirred for an hour. The precipitation products were dried at 100°C for 24 hours and ground in agate mortar. The resulting powders were fired into platinum crucibles at 700°C (in air) for 24 hours in order to release remaining volatiles. Finally, the silica – coated powders were stored in an oven at 120°C. The coated crystalline powders were cold pressed and HIPed for 24 hours at 1150°C and 300 MPa in order to obtain dense and equilibrated melt – bearing polycrystalline samples for deformation. Samples containing 1 and 5 vol. % excess silica glass are called SilLab1 and SilLab5, respectively. SEM investigations were applied to carefully polished and thermally etched specimens (Fig. 1). The microstructure is comparable to those of melt – free samples, with prismatic and lath shaped grains, and with log – normal grain size distributions (Fig. 1d). The intercept method determined mean arithmetic grain sizes of 8.6 ± 3.4 and 9.3 ± 3.2 μm for SilLab5 and SilLab1 samples, respectively. The amorphous phases are more or less homogeneously distributed at multiple grain junctions, as evidenced by SEM in back scattering mode (Fig. 1b). TEM consistently showed that the amorphous phases are present at most multiple grain junctions, with variable apparent dihedral angles. Additionally, most two grain boundaries are wetted by thin amorphous layers < 10 nm in thickness. These features are shown in Figures 2c to 2h. In spite of apparently large dihedral

angles melt films extend from triple junctions within grain boundaries. In addition, the melt film thicknesses gradually increase in the vicinity of the triple junctions, hence suggesting that there are not finite wetting angles. These observations are in part similar to those of Dimanov et al. (2000) for partially molten plagioclase and of Hiraga et al. (2002) for olivine – basalt system, but we did observe some differences too. In the present study we observed that 1) the melt thickness stabilizes at around 10 nm at distances of less than a micrometer from the triple junction, 2) the melt films are a general feature and not exclusively related to low index crystallographic planes as in the latter study. Energy dispersive X ray analysis (EDX) was performed at triple junctions and evidenced that during HIPing the precipitated silica equilibrated chemically with the residual labradorite glass (≈ 1 vol. %), resulting in liquid phases with ≈ 95 ± 2 wt. % and ≈ 85 ± 2 wt. % SiO_2, respectively for SilLab5 and SilLab1 samples (Fig. 2i and 2j, Tab. 1). TEM also evidences the presence of nm scale fluid inclusions in the amorphous phases. FTIR spectroscopy showed similar broad absorption bands and corresponding hydroxyl concentrations (≈ 0.05 ± 0.025 wt. % H_2O) for both melt – bearing and melt – free samples (Fig. 1c). The traces of water could be substantially dried out by annealing in air above 1100°C for 48 hours (Fig. 1c).

2.2. Experimental deformation

Parallelepiped specimens with dimensions of 2.5 mm aside and 5 mm in length were cut from hot pressed samples with low speed diamond saw. Compression and observation surfaces were polished to a finish of 1 μm and 0.3 μm, respectively. Uniaxial creep tests were performed stepwise at constant temperatures and constant loads in a dead – load apparatus (Dimanov et al., 1998; 1999; 2000, 2003). Finite strains for individual steps ranged from 3 to 0.5 %. The details of deformation assemblies and procedures are same as reported in previous works (Dimanov et al., 1998; 1999; 2000). Axial stresses and temperatures were varied stepwise between 3 – 60 MPa and 1100 – 1225°C, respectively. Total sample strain was less than 15 %. Samples were cooled under load. Fast cooling within 10 minutes was only

possible down to 900°C, due to furnace inertial. Further cooling down to room temperature lasted for about two hours. For comparison between static and dynamic conditions, one specimen (lab-04) was only statically annealed at 1200°C, which is an intermediate temperature with respect to the experimental temperature range for the crept samples (Tab. 2, electronic supplement).

3. Results

3.1. Mechanical Data

Stress sensitivity

The mechanical data are provided as electronic supplement (Tab. 2, electronic supplement). All materials showed an extended rage of stress conditions characterized by a linear relation between strain rates and flow stresses (stress exponent n ≈ 1, Fig. 3a,b,c), evidencing linear viscous (Newtonian) flow. A transition to power-low creep (n ≈ 3) could be marginally observed at the highest stresses.

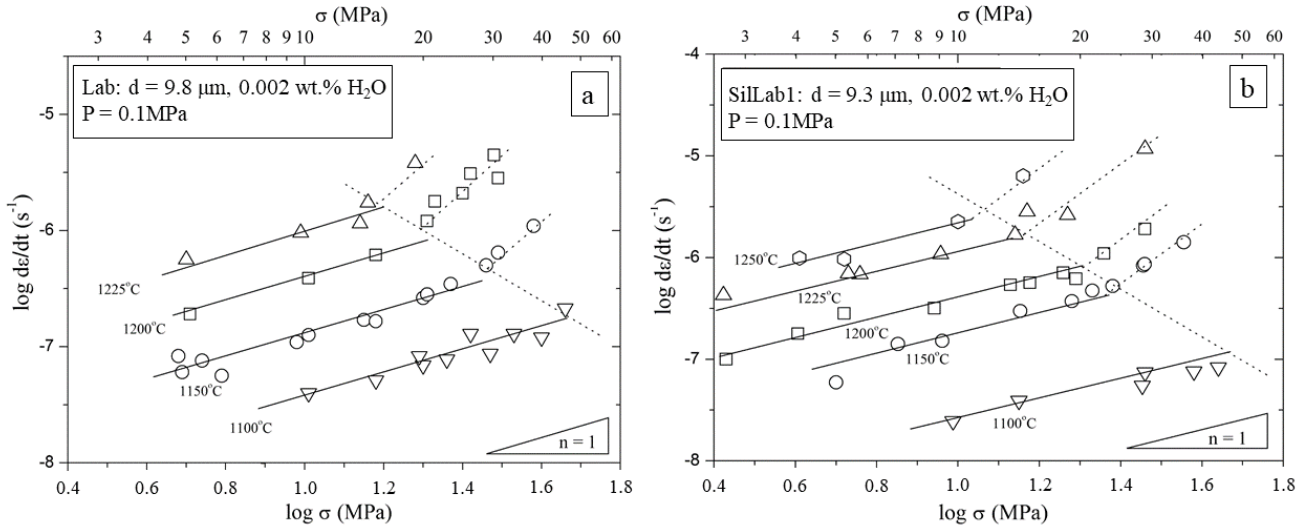

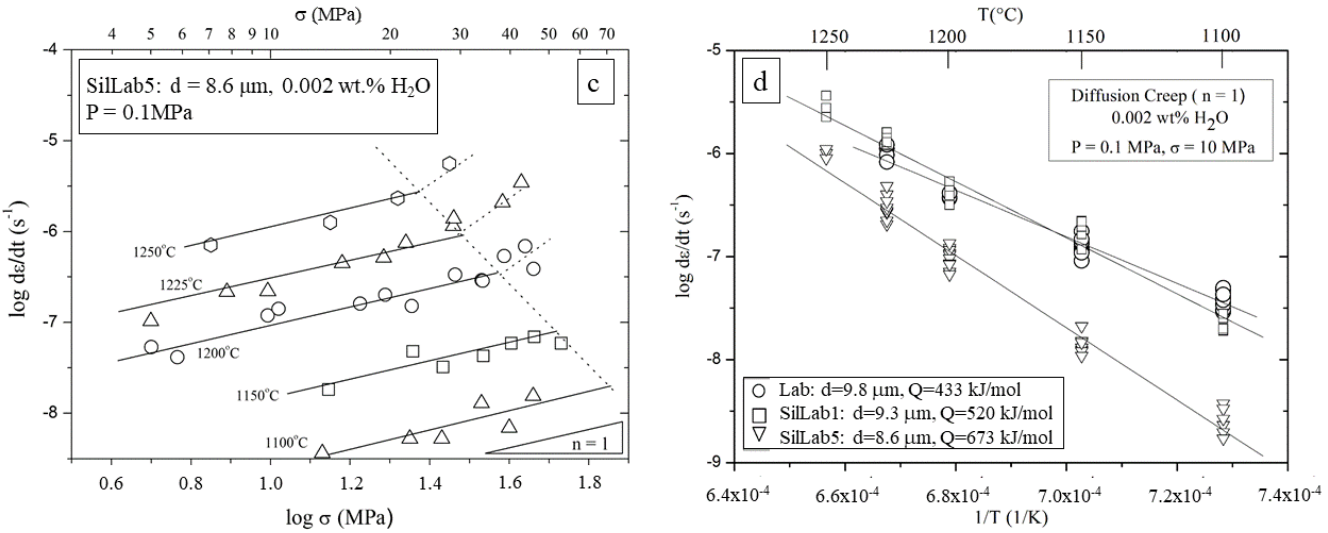

Fig. 3: Thermo-mechanical data for all tested materials. a, b and c: log Stress - log Strain rate plots for Lab, SilLab1 and SilLab5 samples, with respective mean grain sizes of 9.8, 9.3 and 8.6 μm). All materials show dominantly linear viscous (Newtonian) flow (stress exponent n = 1) and a transition (indicated by dot-line) to non-linear behaviour (dislocation creep) at the highest temperatures and stresses, which is in agreement with previous works on similar materials (Dimanov et al., 1998; 1999; 2000). d: Arrhenius diagram of the data for the linear viscous regime for Lab, SilLab1 and SilLab5 samples, recalculated to 10 MPa flow stress showing the Newtonian flow laws. Noteworthy, Lab and SilLab materials present comparable strain rates, whilst SilLab5 material is considerably more resistant. Activation energy increases with melt content.

In this study we are essentially interested in the linear viscous Newtonian flow. Such regimes either relate to Harper-Dorn dislocation-mediated mechanisms, or to grain sliding and/or diffusional mass transfer. In the former and latter cases, the strain rates are respectively grain size sensitive and insensitive. The previous works of Dimanov et al. (1998; 1999; 2000; 2003; 2011) have evidenced for similar materials grain size sensitive flow, which may be described by the constitutive equation:

$$\dot{\varepsilon} = A\,\sigma\, d^{m} e^{-\frac{Q}{RT}} \quad , \qquad (1)$$

where A ($s^{-1}MPa^{-n}\mu m^{m}$) is a material related constant.

Grain size sensitivity

On the one hand, we did not investigate samples with different grain sizes. On the other hand, grain growth was not observed during annealing and creep (Table 2, electronic supplement), possibly because of slow grain boundary migration in the presence of interfacial molten phases. Therefore, we cannot directly measure the dependence of strain rate on grain size. However, a first order estimation may be obtained if we compare the present data for Lab samples (mean grain size $d \approx 10$ μm) with data from Dimanov et al. (1998, 2000). These former data correspond to similar but coarser grained labradorite samples, with mean grain sizes $d \approx 14.5$ μm (Dimanov et al., 2000) and $d \approx 16.5$ μm (Dimanov et al., 1998). We considered exclusively the data corresponding to the Newtonian regime, for temperatures ranging between 1200°C and 1225°C. The data from Dimanov et al. (1998) and from Dimanov et al (2000) correspond respectively to 1213°C and 1210°C (their samples HIP1-01, -02 and -03). The data from the present work correspond to 1200°C and 1225°C (samples lab03 and lab05, Table 2, supplementary data). The activation energies of the flow laws reported by Dimanov et al (2000) and in the present work (396 kJ/mol and 433 kJ/mol, respectively) are comparable within uncertainties. The data from the three studies were reduced to the same flow stress $\sigma = 10$ MPa using $n = 1$, and to an intermediate temperature T = 1213°C using their respective activation energies. A linear regression of the reduced data sets for the three distinct grain sizes yields $m = -2.7 \pm 0.2$ (Fig. 4a), in agreement with previous studies for anorthite plagioclase (Wang et al., 1996; Dimanov et al., 1999) and suggests grain boundary diffusion controlled mechanisms (Coble, 1963).

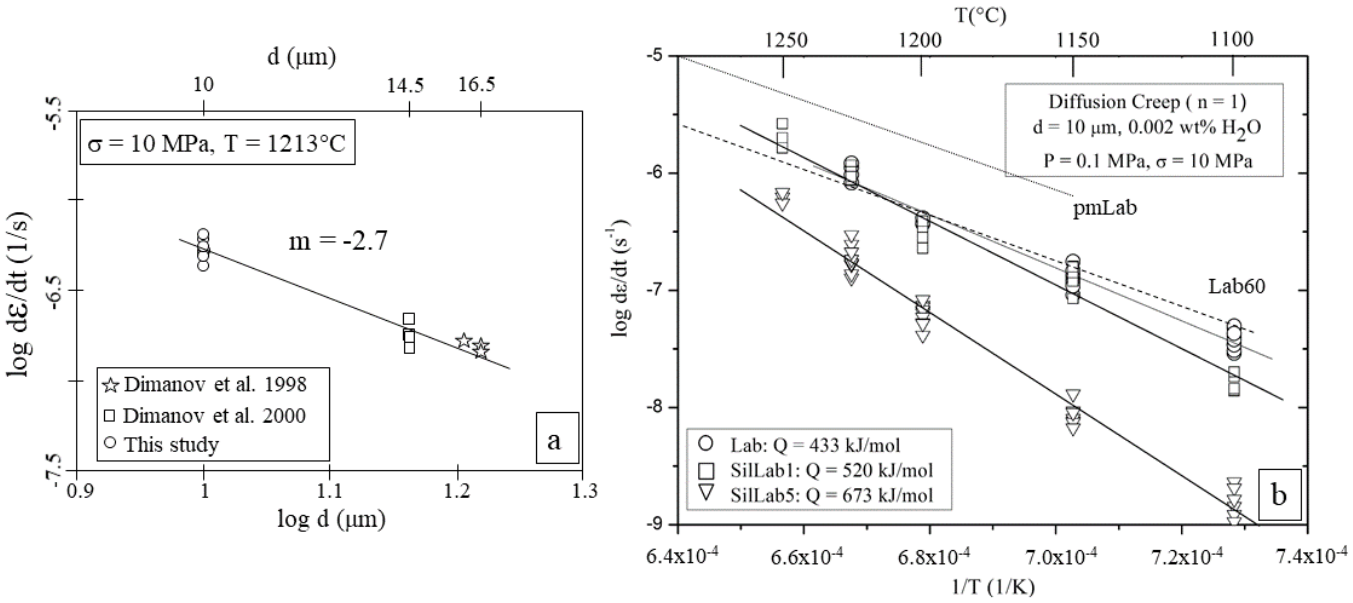

Fig. 4: Thermo-mechanical data for present and previously tested materials. a: log Grain Size - log Strain rate diagram. The data sets are from the present work and from previously published data for similar materials with different grain sizes and reduced to the same flow stress and temperature (see text, Dimanov et al., 1998; 2000). b: Arrhenius diagram, comparing the flow laws for Lab, SilLab1 and SilLab5 materials, for data reduced to the same grain size d = 10 μm. Are reported for comparison previously published flow laws for 1) nominally melt-free labradorite Lab60 containing ca 2 vol. % non-wetting melt from residual glass (comparable to Lab material), 2) partially molten labradorite pmLab containing ca 2 vol. % of residual non-wetting melt, plus ca 1 vol.% of wetting incongruent partial melt with ca 80 wt.% silica (Dimanov et al., 2000).

Considering the former experimental studies, the evidences for grain sliding mechanisms documented by Dimanov et al. (2007) for fine grains anorthite – diopside materials, and the theoretical approach of Ashby and Verall (1973), the present experimental data corresponding to the linear – viscous regime are compatible with the mechanisms of grain sliding accommodated by grain boundary diffusion. In the following, the raw mechanical data will be normalized with respect to grain size with the theoretical value for Coble type of creep: $m = -3$. It is noteworthy that the mean grain sizes for the three materials are not very different, so that the normalization procedure introduces correction factors of respectively ≈ 0.7 and ≈ 0.6 for SilLab5 and SilLab1, which is actually within the experimental scatter. Also, a hypothetical

normalization of mean grain sizes with m = -2 provides corresponding correction factors of 0.9 and 0.7, which do not modify the ground analysis of the experimental results provided in the following.

Activation energy

The parameters of the flow law equation (1) for the different materials Lab, SilLab1 and SilLab5 were obtained by least square regression fits of the respective mechanical data, corresponding to the Newtonian regime (Fig. 3a, 4b, 4c). The results are reported in an Arrhenius diagram (Figure 4b), where the grain sizes for three materials are normalized to a grain size d = 10 μm and to a flow stress σ = 10 MPa using a grain size exponent m = -3 and a stress exponent n = 1. The corresponding flow laws are listed respectively below:

for Lab : $\log A_0$ ($s^{-1}MPa^{-n}$) = 9.03 ± 0.52, n = 1, Q = 433 ± 14 kJ/mol;

for SilLab1 : $\log A_0$ ($s^{-1}MPa^{-n}$) = 12.08 ± 0.76, n = 1, Q = 520 ± 21 kJ/mol;

for SilLab5 : $\log A_0$ ($s^{-1}MPa^{-n}$) = 16.73 ± 0.64, n = 1, Q = 673 ± 18 kJ/mol.

Note the pre-exponential factor A is written as A_0 ($s^{-1}MPa^{-n}$), incorporating the microstructural state variable d (μm). The activation energy and the strain rates for Lab samples are consistent with previously published data for diffusion controlled creep of similar labradorite (Lab60) aggregates (Fig. 4), containing very small amounts of residual non-wetting plagioclase-like melt (Dimanov et al., 1998, 2000). The flow laws for Lab and SilLab1 are nearly identical (Fig. 4). Conversely, SilLab5 samples exhibit substantially lower strain rates and higher activation energy, despite the fact they contain the highest proportion of melt.

Rheological effects of melts

The materials from the present study (Lab) and a previous work (Lab60, Dimanov et al., 2000), containing of 1 – 2 vol. % non-wetting melts (residual starting glass: plagioclase-like composition, with ca 50 wt.% silica) exhibit similar flow laws and are considered as nominally melt-free reference labradorite (Fig. 4). The pmLab material from Dimanov et al. (2000) contains < 2 vol. % of non-wetting residual plagioclase melt plus ca 1 vol. % wetting incongruent partial melt (with 80 wt.% silica) resulting from localized grain boundary pre-melting at hyper solidus conditions. Ii is substantially weaker than the reference labradorite. Conversely, the SilLab1 and SilLab5 materials, containing wetting partial melts with varying compositions (ca 85 and 95 wt. % silica, respectively) exhibit unexpected behaviours. Whilst SilLab1's strength compares to that of Lab material, SilLab5 is substantially stronger, although it contains the highest melt proportion. It is noteworthy that the latter material also exhibits the highest activation energy.

The presence of small amounts of non-wetting partial melt do not strongly influence the diffusion controlled creep laws of labradorite aggregates. In contrast, the presence of small amounts of wetting partial melt have strong but contrasting rheological impacts, which may be either strengthening or weakening. The differences in the rheological effects of the different wetting melts relates to their compositions. Increasing silica content translates in progressive strengthening and increase of activation energy. These observations are discussed in the following at the light of the effects of silica content on polymerization, viscosity and diffusion coefficients of silicate melts.

3.2. Microstructures

Observations of *post mortem* microstructures by SEM did not show noticeable grain growth for both crept and statically annealed specimens (Tab.2, electronic supplement). Deformation did not result in shape preferred orientation. SEM and TEM observations and EDX analysis did not show obvious evolution of melt proportion (within 1 vol. %), topology, or chemistry (within 2 wt. %) during creep. For

Lab samples the small amount of residual glass was never found along grain boundaries. There was no indication for dynamic wetting of grain boundaries as observed sometimes in olivine-basalt assemblages (Jin et al., 1994; Hier-Majumder et al., 2004). For SilLab1 and SilLab5 samples, the initial melt distribution was preserved during deformation: melt still resided at multiple grain junctions and the thin melt films were still present at most grain boundaries. Yet, some evidences for local redistribution of melt along wetted interfaces could be found, in the form of concentric strain contrasts located at wetted grain boundaries (Fig. 5b,c) Studying creep of glass-ceramic systems, Burger et al. (1997) reported the same kind of strain contrast features, that they called “strain whirls”. According to Burger et al. (1997), the latter result from residual elastic strain, corresponding to local stress enhancement associated with the establishment of local dry contacts along previously wetted interfaces. The presence of such localized solid – solid contacts along wetted grain boundaries may be compared with the theoretical island – channel structure proposed by Raj (1982). However, we did not observe massive redistribution or complete melt expulsion out of normally stressed grain boundaries as described for olivine – basalt systems (Jin et al., 1994). Our observations rather support previous authors promoting the stability of thin amorphous interfacial phases, in both static and dynamic conditions (Clarke, 1987; Clarke et al., 1993; Hess, 1994; Drury and FitzGerald, 1996; Wilkinson, 1998).

Curved free dislocations and dislocation arrays could be occasionally observed. Though, consistently with Newtonian viscous flow accommodated by diffusional mass transfer mechanisms, overall dislocation densities, ρ, remained low ($\rho \approx 10^7$ cm^{-2}). Growth twins are very common in undeformed specimens; hence it is difficult to estimate if mechanical twinning could contribute to deformation. In contrast to polished but undeformed samples which simply experienced static thermal etching (see Fig. 1), deformed samples present a strong development of surface topography (Fig. 5). Several previous studies on high temperature uniaxial creep of fine grained materials, such zirconia based ceramic materials (Clarisse et al., 2000; Duclos et al., 2002) and superplastic alloys (Huang and Langdon,

2002), interpreted the development of grain scale topography onto the free surfaces as evidence for grain sliding mechanisms.

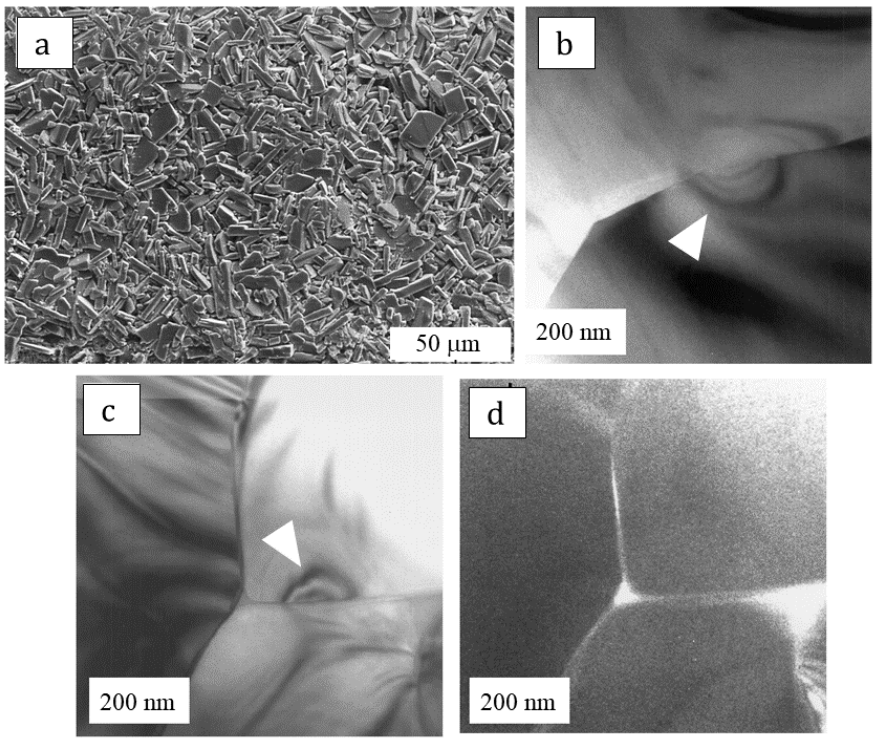

Fig.5: SEM and TEM micrographs of deformed SilLab1 material. a) SEM shows topography development on the sample surface, indicating grain boundary sliding processes. b-c) Bright field images showing dislocation-free grains and whirl shaped strain contrasts (white arrows) next to melt filled pockets (b) or along interfaces (c), which indicate local residual stress related to "dry" contact area (see text). d) Dark field image corresponding to c) showing the presence of amorphous material at interfaces.

4. Discussion

From a general point of view, the mechanical data indicate two dominant creep mechanisms (Figure 4), and thus show show phenomenological similarities with previously reported data for fine grained plagioclase, clinopyroxene and plagioclase-clinopyroxene aggregates (Dimanov et al., 1998; 1999; 2003; Rybacki and Dresen, 2000; Bystricky and Mackwell, 2001; Dimanov and Dresen, 2005; Hier-

Majumder et al., 2005), and olivine aggregates (Hirth and Kohlstedt, 1995; Mei and Kohlstedt, 2000; Mei et al., 2002). From a point of view focussing on the rheological effect of the molten phases, our results present however some striking differences with previous works. To date, all rheological studies of partially molten silicates invariably report melt related weakening, which magnitude depends on melt proportion, grain scale topology and dominant creep mechanisms. Contrastingly, we show that in the case of grain boundary diffusion controlled creep, the presence of extremely silica-rich (95 wt. % SiO_2) wetting melt results in strengthening. Interestingly, zirconia (Kajihara et al., 1995), silicon nitride and silicon carbide ceramics, containing thin amorphous silica films along grain boundaries, systematically exhibit high activation energies and exceptional creep strengths (Meléndez-Martinez and Dominguez-Rodriguez, 2004).

In the specific case of grain boundary diffusional mass transfer, whether wetting partial melts result in weakening or strengthening would be determined by the diffusion properties of the molten phases, which are actually conditioned by their chemical compositions (Zhang et al., 2010). We investigate the effects of melts containing between 80 and 95 wt. % silica, which compositions are close to the end member amorphous silica. At comparable melt content, we observe that the higher is the silica content of the melt and the lower is the strain rates, but the higher is the activation energy.

Diffusivities in silicate melts, and more specifically diffusion rates of network formers as Si, relate to the polymerization degree of the melt. Si diffusion in polymerized Jadeite melt is slow with high activation energy, whilst it is much faster with considerably lower activation energy in depolymerized diopside melt (Shimizu, 1984). The polymerization degree conditions the melt viscocity, and the latter relates to the effective molecular diffusion through the Eyring equation (Ayring, 1936; Glasstone et al., 1941; Mungal, 2002; Nascimento and Zanotto, 2006; Huaiwei et al., 2015):

$$D_{eff} = \frac{k_B T}{\lambda \eta} \quad , \qquad (2)$$

where η is the melt viscosity, D_{eff} is the effective (molecular) diffusivity and λ is the molecular radius. The latter is taken as an approximation for the jump distance of the mobile species or the activated transition state molecular complexes. For complex compositions the effective diffusion coefficient represents the multicomponent (coupled) diffusion of all the constitutive species. The slowest diffusing species, which is rate limiting the coupled diffusion process, remains formally unknown. D_{eff} is however usually considered as a proxy for the self-diffusion coefficients of the basic network formers, namely Si and O (Huaiwei et al. 2015). Experimental investigations show that Si and O have the lowest diffusion rates in dry silicate melts, Si being always the slowest (Zhang et al., 2010). Si is also the slowest diffusing species in silicate minerals (Béjina and Jaoul, 1996; 1997). The Eyring equation (2) is especially applicable to anhydrous and polymerized melts (Shimizu and Kushiro, 1984; Tinker et al., 2004). For O it is convenient at silica contents < 65 wt.%, while for Si it is suited to any composition (Zhang et al., 2010).

Amorphous silica presents a complete tri-dimensional network of SiO_4 tetrahedrons. The major difference with quartz is that its structure is very distorted. Flow of amorphous silica involves transition state molecular complexes within the distorted network of tetrahedrons, which activation involves braking of Si-O bonds. Ojovan and Lee (2004) reported that the formation and the migration enthalpies for such defects to be of 197 and 515 kJ/mol, respectively. The activation energy for silica flow is therefore the summation of the latter values, which is in astonishing agreement with the value we report for creep in SilLab5 samples (673 kJ/mol). Silicon is the primary network former species in silicate melts. Si is therefore most likely the rate limiting species for creep of SiLab5 samples, controlled by diffusion through the silica-rich melt films present at the grain boundaries. However, the investigated melts show varying compositions, with silica contents ranging between 80 and 95 wt.% SiO_2. It is therefore necessary to evaluate their respective diffusion properties, in order to provide quantitative kinetic analysis of the corresponding creep rates. In the following, based on models we will evaluate the viscosities of the silicate

melts present in our samples, from which we will derive the diffusivities of the slowest (rate controlling) species.

4.1. Viscosities of the silicate melts

The viscosity η of a silicate melt depends on the degree of polymerisation of its structural units (Mysen, 1983), which correspond to the network formers species in tetrahedral coordination (in particular Si^{4+} and Al^{3+}, but also Ti^{4+}, Fe^{3+}...). The higher is the polymerization degree and the higher is the concentration of network formers. In opposition, bivalent metals, alkaline and earth alkaline cations represent network modifiers, which decrease the polymerization state, because they relate to non-bridging oxygen within the network of structural tetrahedrons.

Based on a large experimental data sets Giordano et al. (2006, 2008) developed a phenomenological model, which allows to calculate the viscosity of anhydrous silicate melts for temperatures between 700°C and 2000°C, on the basis of their content of network modifiers. The silica richest rhyolitic melt used to derive the phenomenological fitting parameters contained 80 wt. % silica. However, the authors suggested that their model might be applicable for melts containing up to 90 wt. % silica, hence covering the range of compositions for the partial melts of pmLab samples (≈ 80 wt. % SiO_2) and SilLab1 samples (≈ 85 wt. % SiO_2). Lacking any alternative model, we extrapolated the model towards more siliceous compositions to estimate the viscosity for the melt present in our SilLab5 (≈ 95 wt. % SiO_2) samples. Consistently, the calculated viscosities are higher, intermediate and lower for melts present respectively in SilLab5, SilLab1 and pmLab samples, whilst the concerned viscosity range lies between these of pure amorphous silica and albite melt (see appendix A, Fig. A1).

The consistency of the viscosities of the melts present in our samples, calculated with the model of Giordano et al. (2008), may be tested by making a comparison with experimental data as a function of their number of non-bridging oxygen per structural tetrahedron, NBO/T. The latter represents the relative

amounts of network formers and network modifiers, and thus the polymerization degree of a silicate melt. The impurities were neglected and only the major cations (Si, Al, Na, Ca) were taken in account. Al content does not exceed the sum of the charge weighted contents of Na and Ca (Al < Na + 2Ca), and hence Al was entirely assigned to tetrahedral coordination. Following Mysen (1983, 1988; 2003) we calculated NBO/T ≈ 0.01, 0.02 and 0.06 for the melts present in SilLab5, SilLab1 and pmLab materials respectively. The calculated viscosities line up consistently with the experimental ones (see appendix, A, Fig. A1), which indicates that the extrapolation of the model of Giordano et al. (2008) necessary to SilLab5 is reasonable.

4.2. Diffusion coefficients in melts and at grain boundaries

Ion diffusion properties in aluminosilicate melts correlate with their NBO/T and hence correlate inversely with their viscosities (Hofmann, 1980; Shimizu and Kushiro, 1991; Mysen, 1988, Liang et al., 1996). In the temperature range of interest the diffusion rates of network formers Si and Al in silicate melts decrease over many orders of magnitude with increasing silica. This is shown in Figure 6 (and appendix B, Fig. B1), which is a compilation of self-diffusion and inter-diffusion coefficients in silicates materials, considering: i) volume diffusion in single crystals; ii) grain boundary diffusion in polycrystals; iii) diffusion in melts. We restricted to dry systems and to the slowest diffusing network formers (Al, Si and O), which are susceptible to control the kinetics of diffusion controlled creep. In general, diffusion rates of Al, Si and O are way faster at grain boundaries of silicate aggregates than in their single crystal counterparts (Fig. 6 and appendix B, Fig. B1).

Newtonian flow of polycrystalline materials involves bulk diffusion, which operates both in volume and at grain- or interphase boundaries, owing to their specific crystallographic structural defects. The slowest volume diffusion rates relate to point defects (vacancies, interstitials, substitutional impurities and their associations). Alternatively, faster volume diffusion may operate through shortcuts provided by

extended linear defects (dislocation and dislocation arrays) and planar defects (low angle– or sub–grain boundaries), Grain boundary diffusion rates along high angle grain boundaries are usually much faster than volume diffusion, because grain boundaries are themselves two dimensional crystallographic defects, presenting the largest crystallographic deviations from bulk crystal structure. Volume diffusion coefficients in plagioclases are several orders of magnitude slower than grain boundary diffusion coefficients in similar materials. As far as concerned with diffusion controlled mass transfer and creep, strain rates are controlled by the slowest diffusing species diffusing through the fastest pathway. Accordingly, the creep rates of nominally crystalline plagioclase would be controlled by grain boundary diffusion rates. Consistently, the grain size exponent we derived from creep of nominally melt-free labradorite indicate grain boundary diffusion control. The creep rates of partially molten labradorite are also likely governed by diffusion along grain boundaries wetted by melt. The presence of melt films wetting grain boundaries would in principle modify the diffusional mass transfer mechanisms, switching from grain boundary diffusion to diffusion through the melt. The net result on the mass transfer kinetics would depend on the ratio of the diffusion coefficient in the melt relative to the grain boundary diffusion coefficient. This is to say the effective diffusivities would be strongly conditioned by the melt composition. Indeed, diffusion rates in melts are very fast in basalts, intermediate in rhyolitic melts and substantially slow in plagioclase melts (Fig. 6). Noteworthy, the extremely low self-diffusion coefficient of Si in pure amorphous silica is nearly comparable with that in pure single crystal quartz, which reflects the similarity of the polymerized tri-dimensional network of SiO_4 tetrahedrons in both materials.

The calculated viscosities of the melts wetting grain boundaries in pmLab, SilLab1 and SilLab5 samples (see appendix A, Fig. A1) can be interpreted in terms of effective diffusivities, D_{eff}, based on equation (2) and taking $\lambda = 10^{-10}$ m as a first order approximation. The results are convincingly consistent when compared with appropriate experimental data (Fig. 6 and appendix B, Fig.B1): the calculated effective diffusion coefficients are intermediate between volume diffusion and grain boundary diffusion

in silicates. Alternatively, if we use for equation (2) $\lambda \approx 0.3$ nm, which is the effective radius for oxygen (Shannon, 1976), the effective diffusion coefficients would be lower with about half an order of magnitude. It is noteworthy that grain boundary diffusion rates in plagioclase were estimated from the kinetics of reaction rim growth in wet conditions (Liu et al., 1997; Yund, 1997; Yund and Farver, 1999; Milke et al., 2001; Abart et al., 2004). However, direct comparison cannot be done with our data, corresponding to dry conditions. Alternatively, the existing grain boundary diffusion data for other dry silicates, oxides and aluminosilicates (dotted lines) match reasonably with the slowest diffusivities in the most polymerized aluminosilicate melts (rhyolite, albite).

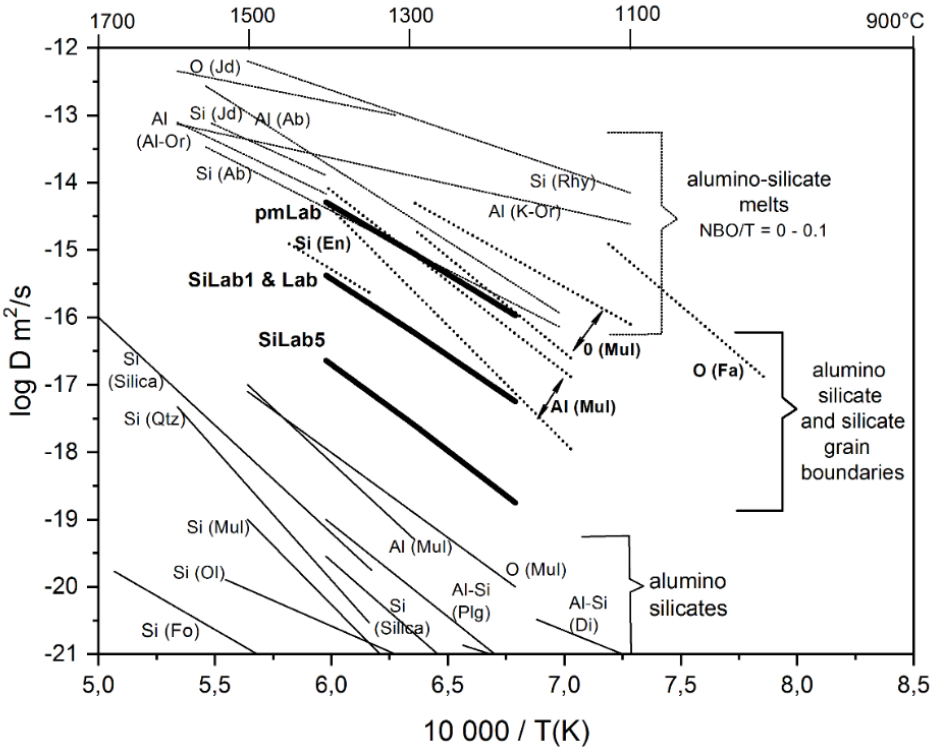

Fig. 6: Arrhenius diagram of volume and grain boundary diffusion of network formers (Si, Al and O) in silicates and oxides and in silicate melts (in dry or unsaturated conditions). The data are recalculated for a pressure of 0.1 MPa (when activation volumes were available). Bas is basalt, Rhy is rhyolitic melt, Di and Jd refer to diopside and jadeite melts, Ab and KAS are albite and potassium-aluminosilicate melts. Diffusivity of Si in silica falls within the lower field for volume diffusion. Diffusivities of O in silica fall in-between the two fields. Grain boundary diffusivities (recalculated for a grain boundary width of ~ 3 nm) are represented by heavy dot lines. The larger vertical brackets indicate the type of diffusivity. For diffusion in

melt the smaller brackets indicate the compositional ranges and the corresponding NBOT numbers. The diffusivities calculated for our melt compositions (see text) are reported as heavy lines and compared to existing grain boundary diffusivities (light dotted lines) in aluminosilicates and silicates (Mulite: Mul, Enstatite: En, Fayalite: Fa) and calculated diffusivities for the present highly polymerized aluminosilicate melts (pmLab, SilLab1 and SilLab5). It appears that grain boundary diffusivities are in general comparable to the lowest diffusivities in alumino-silicate melts, as do the diffusivities for pmLab and SilLab1 melts. The diffusivity for SilLab5 melt shows however substantially lower, in-between the lowest diffusivities in alumina-silicate melts and the highest diffusivities in alumina-silicate single crystals. The references for the diffusion data are reported in appendix B, Figure B1.

The calculated D_{eff} for the albitic–like melt in pmLab samples (containing ca 80 wt. % silica) matches nearly perfectly the measured Si diffusivity in albite melt (ca 70 wt. % silica), which supports our approach to determine diffusivity from viscosity estimates and the Eyring equation. Consistent with the dependence of Si self–diffusion on silica content in silicate melts (Zhang et al., 2010), the calculated effective diffusivities decrease monotonously from pmLab–melt to SilLab1–melt, and to SilLab5–melt. The faster D_{eff} for pmLab melt exceeds by about an order of magnitude grain boundary diffusivities in silicates and oxides (enstatite, alumina and mulite), which is fully consistent with the observation that the strain rates for pmLab samples are about an order of magnitude faster than those for nominally melt–free Lab and Lab60 materials. Intermediate D_{eff} for SilLab1 melt mimics grain boundary diffusion rates for dry silicates, oxides and aluminosilicates, consistent with strain rates for SilLab1 samples comparable to those for nominally melt-free Lab and Lab60 materials. Conversely, D_{eff} for SilLab5 type of melt (95 wt. % silica) is much lower than the self-diffusion coefficients of Si, Al and O in any of the usually investigated silicate melts (with < 80 wt.% silica). D_{eff} decreases by about two and half orders of magnitude between pmLab melt and SilLab5 melt. Figure 6 also shows that D_{eff} for SilLab5 melt is substantially lower than any of the reported grain boundary diffusion coefficients for Si, Al and O. From the perspective of grain boundary diffusion creep, these observations are consistent with the finding that strain rates for Sillab5 are considerably lower than those for nominally melt–free (Lab and Lab60) and

for SilLab1 materials. In summary, on the one hand our findings suggest that thin melt films of polymerized wetting melt (ca. 85 wt.% silica) do not noticeably affect grain boundary diffusion coefficients with respect to crystalline grain boundaries. On the other hand, albitic–like wetting melt (ca 80 wt.% silica) considerably enhance the effective grain boundary diffusion coefficients. Conversely, the latter are strongly decreased by the presence of extremely polymerized wetting melt (ca 95 wt.% silica).

4.3 Implications

Extremely silica–rich melts are not very common, but may be found in a few geodynamic contexts. Hydrothermal weathering and preferential leaching processes of silicate minerals may result in the formation of small amounts of siliceous amorphous phases (Eggleton and Smith, 1983; Ruiz-Agudo et al., 2012; Hellmann et al, 2013; Daval et al., 2018; Wild et al., 2019). Some unusually quartz–rich granites originate from very silica–enriched melts (Chen et al., 2021), whilst some crustal xenoliths exhibit silica-rich melt inclusions (Frezzotti et al. 2004). Low degree of melting of some mantle xenoliths may result in the generation of very silica–rich amorphous phases, which are either preserved as volume inclusions (Schiano et al., 1995), or as glassy grain boundary films (Wirth, 1996; Franz and Wirth, 1997). Conversely, experiment approaches report low degree of localised melting in relation to stress state or chemical environment. Samae et al. (2021) report on stress related grain boundary amorphization. The evolution of point defect populations in iron–bearing diopside may result in lattice precipitation of a few vol. % of nearly pure silica droplets; a process called early partial melting (Raterron and Jaoul, 1991; Ingrin et al., 1991; Doukhan et al., 1993, Raterron et al., 1995). From a more general perspective on partially molten silicates our work demonstrates that melt composition may have strong influences on mass transfer kinetics, and hence on transport properties involved in creep, but also in electrical conductivity. Depending on the different geodynamic contexts resulting in low degree of melting, the mechanical behaviour of the resulting partially molten rocks must also be considered from the point of

view of melt chemistry. However, our work focussed exclusively on dry systems. The role of aqueous species in depolymerisation of silicate melts and enhancement of diffusion coefficients is well–known (Brady, 1995, Zhang et al., 2010). Therefore, complementary work would be necessary to investigate the rheological effects of melt chemistry in water bearing silicate systems.

5. Conclusions

We studied the high-temperature rheology of nominally melt-free and partially molten plagioclase aggregates by uniaxial creep at dry conditions. The synthetic fine grained materials (ca 10 μm grain size) contain less than 6 vol. % silica-rich melt, of which less than 1 vol. % resides as thin films (< 10 nm) at numerous grain boundaries. The mechanical data show dominant linear viscous rheology. The microstructures and the strong grain size sensitivity (grain size exponent m = -2.7) indicate grain boundary sliding controlled by grain boundary diffusional mass transfer. We specifically focussed on the effect of the composition of the wetting melt on the latter controlling mechanisms. Varying the silica content of the wetting melts between 80 and 95 wt. % silica, we demonstrated a strong impact of melt chemistry on the diffusion controlled Newtonian rheology. Samples containing melts with ca 80, 85 and 95 wt. % silica were respectively weaker, comparable, and substantially stronger than nominally melt-free samples. The activation energy for the stronger material was also considerably higher than for the other materials. Based on existing models, we estimated the viscosities of the silica-rich melts and the effective diffusivities for their slowest constitutive species. The calculated values are consistent with experimental viscosity and diffusion data. Regarding the progressively decreasing effective diffusivity with increasing silica content of the silica-rich melts, we interpret the relative weakening or strengthening effects for our partially molten samples as respectively representative of enhanced or hindered diffusion properties through the thin melt films wetting grain boundaries.

Acknowledgements

The author is grateful to R.C. Cooper for kindly providing the starting glass powder, and to J. Huang and M. Naumann who assisted with sample preparation techniques and mechanical testing. R. Wirth and E. Rybacki are acknowledged for TEM observations and for many stimulating discussions. G. Dresen is warmly thanked for proving unlimited access to his experimental facilities and for his unconditional support. The comments and suggestions of two anonymous reviewers helped to improve and clarify the manuscript.

Data Availability

The experimental data are available.

References

Abart, R., Kunze, K., Milke, R., Sperb, R. and Heinrich, W., (2004), Silicon and oxygen self-diffusion in enstatite polycrystals: the Milke et al. (2001) rim growth experiments revisited. Contrib. Mineral. Petrol., Vol. 147, 633-646.

Ashby, M.F. and Verall, R.A. (1973), Diffusion accommodated flow and superplasticity. Acta Metallurgica. Vol. 21, 149-163.

Eyring, H. (1936) Viscosity, plasticity, and diffusion as examples of absolute reaction rates. J. Chem. Phys., 4, 283–291.

Baker, D.R., (1990), Chemical interdiffusion of dacite and rhyolite: anhydrous measurement at 1 atm and at 10 kbar, application of transient state theory and diffusion in zoned magma chambers. Contrib. Mineral. Petrol., Vol.104: 407-423.

Baker, D.R., (1992), Tracer diffusion of network formers and multicomponent diffusion in dacitic and rhyolitic melts. Geochim. Cosmochim. Acta., Vol. 56, 462-473.

Baker, D.R., (1995), Diffusion of silicon and gallium (as an analogue for aluminum) network-forming cations and their relationship to viscosity in albite melt. Geochim. Cosmochim. Acta., Vol. 59 (17), 3561-3571.

Beeman M.L. and Kohlstedt, D.L. (1993), Deformation of Fine-Grained Aggregates of Olivine Plus Melt at High Temperatures and Pressures. J. Geophys. Res., Vol. 98, B4, 6443-6452, doi:10.1029/92JB02697

Beere, W. (1975), The second stage of sintering of powder compacts. Acta Metal. 23(1), 139-145.

Béjina, F. and Jaoul, O., (1996), Silicon self-diffusion in quartz and diopside measured by nuclear micro-analysis methods. Phys. Earth. Planet. Interiors, Vol. 97, 145-162.

Béjina, F. and Jaoul, O. (1997), Silicon diffusion in silicate minerals. EPSL, Vol. 153 (3-4), 229-238. DOI:10.1016/S0012-821X(97)00190-8

Beran, A., (1986), A model of Water Allocation in Alkali Feldspar, Derived from Infrared-Specroscopic Investigations. Phys. Chem. Minerals, Vol. 13, 306-310.

Beran, A., (1987), O.H. Groups in Nominally Anhydrous Framework Structures: An Infrared Spectroscopic Investigation of Danburite and Labradorite. Phys. Chem. Minerals, Vol.14, 441-445.

Brady, J.B. (1995) Diffusion data for silicate minerals, glasses, and liquids. In: Ahrens T.J. (Ed.) Mineral Physics and Crystallography. A Handbook of Physical Constants 2, AGU Reference Shelf 2, Washington DC, 269-290.

Brebec, G., Seguin, R., Sella, C., Benevot, J. and Martin, J.C., (1980), Diffusion du silicium dans la silice amorphe. Acta Metall., Vol. 28, 327-333.

Bulau, J.R., Waff, H.S. and Tyburczy, J., (1979), Mechanical and thermodynamic constraints on fluid distribution in partial melts. J. Geophys. Res., vol. 84, B11, 6102-6108.

Burger, P., Duclos, R. and Crampon, J., (1997), Microstructure characterization in superplastically deformed silicon nitride. J. Am. Ceram. Soc., Vol. 80, 879-885.

Bussod, G.Y and Christie J.M. (1991), Textural development and melt topology in spinel lherzolite experimentally deformed at hypersolidus conditions. J. Petrol. Special lherzolite issue, 17–39.

Bystricky, M., and S. Mackwell (2001), Creep of dry clinopyroxene aggregates, J. Geophys. Res., Vol. 106, 13443-13454.

Canil, D. and Muehlenbachs, K., (1990), Oxygen diffusion in an Fe-rich basalt melt. Geochim. Cosmochim. Acta., Vol. 54: 2947-2951.

Carapic, G., Faul, U.H. and Brisson, E. (2013), High-resolution imaging of the melt distribution in partially molten upper mantle rocks: evidence for wetted two-grain boundaries. Geochem. Geophys. Geosyst., Vol. 14(3), 556-566 doi:10.1029/2012GC004547.

Chakraborty, S., Dingwell, D.B. and Rubie, D.C., (1995), Multicomponent diffusion in ternary silicate melts in the system K_2O-Al_2O_3-SiO_2: II. Mechanisms, systematics, and geological implications. Geochim. Cosmochim. Acta., Vol. 59(2), 265-277.

Chen, J.-Y; Yang, J.-H.; Zhang, J.-H.; Sun, J.-F.; Zhu, Y.-S. and Hartung E. (2021), Generation of Cretaceous high-silica granite by complementary crystal accumulation and silicic melt extraction in the coastal region of southeastern China. GSA Bulletin (2021) https://doi.org/10.1130/B35745.1

Clarisse L., Petit F., Crampon J. and Duclos R., (2000), Characterization of grain boundary sliding in a fine-grained alumina-zirconia ceramic composite by atomic force microscopy. Ceram. Int., Vol. 26(3), 295-302.

Clarke, D.R., (1987), On the equilibrium thickness of intergranular glass phases in ceramic materials. J. Am. Ceram. Soc., Vol. 70, 15-22.

Clarke D.R., Shaw, T.M., Philipse, A.P. and Horn, R.G. (1993), Possible electrical double layer contribution to the equilibrium thickness of intergranular glass films in polycrystalline ceramics. J. Am. Ceram. Soc., Vol. 76(5), 1201-1204.

Cmíral, M., Fitz Gerald, J.D., and Faul, U.H., (1998), A close look at dihedral angles and melt geometry in olivine-basalt aggregates: a TEM study, Contib Minearal Petrol, Vol.130, 336-345.

Coble, R.L., (1963), A model for boundary diffusion controlled creep in polycrystalline materials. J. Appl. Phys., Vol. 34, 1679-1682.

Cooper, R.F. and Kohlstedt, D.L., (1984), Solution - precipitation enhanced diffusional creep of partially molten olivine-basalt aggregates during hot-pressing. Tectonophysics, Vol. 107, 207-233.

Cooper, R.F. and Kohlstedt, D.L., 1986. Rheology and Structure of Olivine - Basalt Partial Melts. J. Geophys. Res. Vol. 91, B9, 9315-9323.

Cooper, R.F., Kohlstedt, D.L. and Chyung. K., (1989), Solution-precipitation enhanced creep in solid-liquid aggregates which display a non-zero dihedral angle. Acta Metall., Vol. 37, 1759-1771.

Daines, M.J. and Kohlstedt, D.L., (1997), Influence of deformation on melt topology in peridotites. J. Geophys. Res., Vol. 102, B5, 10257-10271.

Daval, D. ; Calvaruso, C. ; Guyot, F. ; Turpault, M.-P. (2018) Time-dependent feldspar dissolution rates resulting from surface passivation: Experimental evidence and geochemical implications. Earth and Planetary Science Letters, Volume 498, p. 226-236. 10.1016/j.epsl.2018.06.035

Dell'Angelo, L.N. and Tullis, J., (1988), Experimental deformation of partially melted granitic aggregates. J. Metamorph. Geol., Vol. 6, 495-515.

Dell'Angelo, L.N., Tullis, J. and Yund, R.A., (1987), Transition from dislocation creep to melt-enhanced diffusion creep in fine grained granitic aggregates. Tectonophysics, Vol. 139, 325-332.

Dimanov, A., Dresen, G. and Wirth, R., (1998), High-temperature creep of partially molten plagioclase aggregates. J. Geophys. Res., Vol. 103, B5, 9651-9664.

Dimanov, A., Xiao, X., Dresen G. and Wirth. R., (1999), Grain Boundary Diffusion Creep of Synthetic Anorthite: The Effect of Water. J. Geophys. Res., Vol. 104, 10483-10497.

Dimanov, A., Wirth, R. and Dresen, G., (2000), The effect of melt distribution on the rheology of feldspar rocks. Tectonophysics, Vol. 328, 307-327.

Dimanov, A., Lavie, M.P., Ingrin, J., Dresen, G. and Jaoul, O. (2003), Creep of polycrystalline anorthite and diopside. J. Geophys. Res. Vol. 108, B1, 2061, doi:10.10292002JB001815.

Dimanov, A., Rybacki, E., Wirth, R. and Dresen G. (2007), Creep and strain-dependent microstructures of synthetic anorthite-diopside aggregates: J. Struct. Geol., Vol. 29, 1049–1069, doi: 10.1016/j.jsg.2007.02.010.

Dimanov, A., Raphanel, J. and Dresen G. (2011), Newtonian flow of heterogeneous synthetic gabbros at high strain: Grain sliding, ductile failure, and contrasting local mechanisms and interactions. Eur. J. Min., Vol. 23(3), 303-322, doi: 10.1127/0935−1221/2011/0023−2110

Dimanov A. and Dresen, G. (2005), Rheology of synthetic anorthite-diopside aggregates: Implications for ductile shear zones. J. Geophys. Res., Vol. 110, doi:10.1029/2004JB003431.

De Kloe, R., Drury, M.R., and van Roermund, H.L.M., (2000), Evidence for stable grain boundary melt films in experimentally deformed olivine –orthopyroxene rocks, Phys Chem Minerals, Vol. 27, 480-494.

Doukhan, N., Doukhan, J.C., Ingrin, J., Jaoul, O., and Raterron, P. (1993) Early partial melting in pyroxenes. Am. Mineral., 78: 1246-1256.

Drury, M.R. and FitzGerald, J.D., (1996), Grain boundary melt films in an experimentally deformed olivine-orthopyroxene rock: implications for melt distribution in upper mantle rocks. Geophys. Res. Lett., Vol. 23(7), 701-704.

Duclos, R., Crampon, J. and Carry, C., (2002), Grain-boundary sliding and accommodation mechanism during creep of yttria-partially-stabilized zirconia. Philos. Mag. Lett., Vol. 82(10), 529-533.

Eggleton, R.A and K. L Smith (1983), Silicate alteration mechanisms. Sciences Géologiques, bulletins et mémoires vol 71 pp. 45-53

Ruiz-Agudo, E.; Putnis, C.V.; Rodriguez-Navarro, C. and Putnis, A. (2012) Mechanism of leached layer formation during chemical weathering of silicate minerals. Geology 40 (10): 947–950. https://doi.org/10.1130/G33339.1

Fielitz, P., G. Borchardt, M. Schmüker, H. Schneider and P. Willich (2004), Oxygen grain-boundary diffusion in polycrystalline Mullite Ceramics. J. Am. Ceram. Soc., Vol. 87(12), 2232-2236. doi: 10.1111/j.1151-2916.2004.tb07497.x

Fielitz, P., G. Borchardt, M. Schmüker and H. Schneider (2007), A diffusion-controlled mullite formation reaction model based on tracer diffusivity data for aluminium, silicon and oxygen. Phil. Mag., Vol. 87(1), 111-127.

Fielitz,P. and G. Borchardt (2016), Self-Diffusion of the Constituent Elements in Alpha-Alumina, Mullite and Aluminosilicate Glasses", Diffusion Foundations, Vol. 8, 80-108.

Fisler, D.K. and Mackwell, S.J., (1994), Kinetics of diffusion-controlled growth of fayalite. Phys. Chem. Minerals, Vol. 21, 156-165.

Fisler, D.K., Mackwell, S.J. and Petsch, S., (1997), Grain boundary diffusion in enstatite. Phys. Chem. Minerals, Vol. 24, 264-273.

Franz, L. and Wirth, R., (1997), Thin intergranular melt films and melt pockets in spinel peridotite xenoliths from the Rhön area (Germany): early stage of melt generation by grain boundary melting. Contrib. Mineral. Petrol., Vol. 129 (4), 268-283.

Frezzotti, M-L, A., Peccerillo, V., Zanon and I., Nikogosian (2004), Silica-rich Melts in Quartz Xenoliths from Vulcano Island and their Bearing on Processes of Crustal Anatexis and Crust-Magma Interaction beneath the Aeolian Arc, Southern Italy. J. Petrol., Vol. 45 (1), 3-26. DOI: 10.1093/petrology/egg080

Fujii, N., Osamura, K. and Takahashi, E. (1986), Effect of water saturation on the distribution of partial melt in the olivine-pyroxene-plagioclase system. J. Geophys. Res., Vol. 91, 9253-9259.

Giordano, D., Mangicapra, A., Potuzak, M., Russell, J.K., Romano, C., Dingwell, D.B. and Di Muro, A. (2006), An expanded non-Arrhenian model for silicate melt viscosity: A treatment for metaluminous, peraluminous and peralkaline melts. Chem. Geol., Vol. 229, 42–56.

Giordano, D., Russell, J.K. and Dingwell, D.B. (2008), Viscosity of magmatic liquids: a model. Earth and Planet. Sci. Letts., Vol. 271, 123-134.

Glasstone, S., Laidler, K. J. and Eyring, H. (1941) The Theory of Rate Processes, pp. 611, McGraw-Hill, New York.

Grove, T.L., Baker, M.B. and Kinzler, R.J., (1984), Coupled CaAl - NaSi diffusion in plagioclase feldspar: experiments and applications to cooling rate speedometry. Geochim. Cosmochim. Acta., Vol. 48, 2113-2121.

Hamilton, D.L., and Henderson, C.M.B. (1968), The preparation of silicate compositions by a gelling method. Mineral. Mag., Vol. 36, 832-838.

Harmer M.P. and Brook R.J., (1980), The effect of MgO additions on the kinetics of hot pressing in Al_2O_3. J. Mater. Sci., Vol. 15, 3017-3024.

Harris, N. (2007), Channel flow and the Himalayan–Tibetan orogen: a critical review, *J. Geol. Soc.*, Vol. 164(3), 511-523, doi: 10.1144/0016-76492006-133

Hellmann, R.; Daval, D. and Wirth, R. (2013) Formation of Amorphous Silica Surface Layers by Dissolution-Reprecipitaton During Chemical Weathering: Implications for CO2 Uptake, Procedia Earth and Planetary Science 7:346–349, DOI:10.1016/j.proeps.2013.03.154

Hess, P.C., (1994), Thermodynamics of thin fluid films. J. Geophys. Res., Vol. 99, B4, 7219-7229.

Hetherington, G., Jack, K.H. and Kennedy, J.C. (1964), The viscosity of vitreous silica. Phys. Chem. Glass., Vol. 5, 130-136.

Hier-Majumder, S., P.H. Leo and D.L. Kohlstedt (2004), On grain boundary wetting during deformation. Acta Mater. Vol. 52, 3425-3433, doi:10.1016/j.actamat.2004.03.040

Hier-Majumder, S., S. Mei, and D.L. Kohlstedt (2005), Water weakening of clinopyroxene in the diffusion creep regime, J. Geophys. Res. Vol. 110, B07406, doi:10.1029/2004JB003414

Hiraga, T., Anderson, I., Zimmerman, M., Mei, S. and Kohlstedt, D. (2002), Structure and chemistry of grain boundaries in deformed, olivine + basalt and partially molten lherzolite aggregates: evidence of melt-free grain boundaries. Contrib. Mineral. Petrol., Vol.144, 163-175, doi:10.1007/s00410-002-0394-1

Hirth, G. and Kohlstedt, D.L., (1995), Experimental constraints on the dynamics of the partially molten upper mantle: Deformation in the diffusion creep regime. J. Geophys. Res., Vol. 100, B2, 1981-2001.

Hofmann, A.W. (1980), Diffusion in silicate melts: a critical review. In Physics of Magmatic Processes (ed. R.B. Hargraves), 385-417. Princeton Univ. Press.

Hofmeister, A. and Rossman, G., (1985), A model for the Irradiative Coloration of Smoky Feldspar and the Inhibiting Influence of Water. Phys. Chem. Mineral., Vol. 12: 324-332.

Holtzman B.K. and Kohlstedt D.L., (2007), Stress driven melt segregation and strain partitioning in partially molten rocks: Effects of stress and strain. J. Petrol., Vol. 48, 2379-2406.

Houlier, B., Cheraghmakani, M., Jaoul, O., (1990), Silicon diffusion in San-Carlos olivine. Phys. Earth Planet. Interiors., Vol. 62, 329-340.

Huaiwei, Ni, Hejiu Hui, and Gerd Steinle-Neumann (2015) Transport properties of silicate melts. Reviews of Geophysics, Vol. 53(3), 715-744 https://doi.org/10.1002/2015RG000485.

Huang, Y. and Langdon, T.G. (2002), Characterization of deformation processes in a Zn-22% Al alloy using atomic force microscopy. J. Mat. Sci., Vol. 37(23), 4993-4998.

Ildefonse, B. and Nicolas, B. (1997), Ecoulement magmatique dans les gabbros et problème des chambres magmatiques sous les dorsales océaniques. In "Des grands écoulements naturels à la dynamique du tas de sable : introduction aux suspensions concentrées en géologie et en physique" (B. Ildefonse, C. Allain & P. Coussot, eds.), Cemagref Editions, 37-49.

Ingrin, J., Doukhan, N., and Doukhan, J.C., 199 1. High-temperature of diopside single crystal 2: Transmission electron microscopy investigation of the defect microstructures. J. Geophys. Res., 96: 14,287-14,297.

Jaoul, O., Poumellec, M., Froidevaux, A. and Havette, A., (1981), Silicon diffusion in forsterite: a new constraint for understanding mantle deformation. In Anelasticity in the Earth (Stacey FD, Paterson MS and Nicolas A, Eds.), AGU Geodyn. Ser. Vol. 4, 95-100.

Jaoul, O., Sautter, V. and Abel, F. (1991), Nuclear microanalysis: A powerful tool for measuring low atomic diffusivity with mineralogical applications. In "Advances in Physical Geochemistry, Diffusion, Atomic Ordering, and Mass Transport: Selected Problems in Geochemistry", J. Ganguly, ed., Springer-Verlag, Berlin, Vol. 6, 198-200.

Jin, Z.M., Green, H.W. and Zhou, Y. (1994), Melt topology in partially molten mantle peridotite during ductile deformation. Nature, Vol. 372, 164-167.

Jung, H. and Waff, H.S. (1998), Olivine crystallographic control and anisotropic melt distribution in ultramafic partial melts. Geophys. Res. Lett., Vol. 25, 2901-2904.

Jurewitz, S. R. and E. B. Watson (1985), The distribution of partial melt in a granitic system: the application of liquid phase sintering theory. geochim. Cosmochim. Acta, Vol. 49, 1109-1121.

Kajihara, K., Yoshizawa, Y. and Sakuma, T. (1995), The enhancement of superplastic flow in tetragonal zirconia polycrystals with SiO_2-doping. Acta Metall. Mater. Vol. 43, 1235-1242.

Katz R.F., Spiegelman M. and Holtzman B. (2006), The dynamics of melt and shear localization in partially molten aggregates, Nature, Vol. 442, 676-679.

Kohlstedt, D.L. (1992), Structure, Rheology and permeability of partially Molten Rocks at Low Melt Fractions. Mantle Flow and Melt Generation at Mid - Ocean Ridges. AGU Geophys. Monograph Vol. 71, 10-121.

Kohlstedt, D.L. and Zimmermann, M.E. (1996), Rheology of partially molten mantle rocks. Annu. Rev. Earth Planet. Sci., Vol. 24, 41-62.

Kress, V.C. and Ghiorso, M.S. (1995), Multicomponent diffusion in basaltic melts. Geochim. Cosmochim. Acta. Vol. 59(2) 313-324.

Lamoureux, G., B. Ildefonse, and D. Mainprice (1999), Modelling the seismic properties of fast-spreading ridge crustal LVZ: insights from Oman gabbro textures. Tectonophysics, Vol. 312, 283–301.

Laporte, D. and Watson, E.B. (1995), Experimental and theoretical constraints on melt distribution in crustal sources: the effect of crystalline anisotropy on melt interconnectivity. Chem. Geol., Vol. 124, 161-184.

Laporte, D., Rapaille, C. and Provost, A. (1997), Wetting angles, equilibrium melt geometry, and the permeability threshold of partially molten crustal protoliths. In Granite: from segregation of melt to emplacement fabrics. (ed. J.L. Bouchez), Kluwer Academic Publishers, Netherlands, 31-54.

Le Gall, M., Lesage, B. and Bernardini, J. (1994), Self-diffusion in alpha-Al2O3. 1. Aluminium diffusion in single-crystals. Philos. Mag. A, Vol. 70(5), 761-773.

Lesher, C.E., Hervig, R.L. and Tinker, D. (1996), Self-diffusion of network formers (silicon and oxygen) in naturally occuring basaltic liquid. Geochim. Cosmochim. Acta. Vol. 60(3), 405-413.

Liang, Y., Richter, F.M., Davis, A.M. and Watson, B. (1996), Diffusion in silicate melts: I. Self-diffusion in CaO – Al2O3 – SiO2 at 1500°C and 1 GPa. Geochim. Cosmochim. Acta., Vol. 60, 4353-4367.

Liu, M., Peterson, J.C. and Yund, R.A. (1997), Diffusion-controlled growth of albite and pyroxene reaction rims. Contrib. Mineral. Petrol., Vol. 126, 217-223.

Mecklenburgh, J. and Rutter, E.H. (2003), On the rheology of partially molten synthetic granite. J. Struct. Geol., Vol. 25, 1575-1585.

Meléndez-Martinez, J.J. and Dominguez-Rodriguez, A. (2004), Creep of silicon nitride. Prog. Mat. Sci., Vol. 49, 19-107.

Mei, S. and Kohlstedt, D.L. (2000), Influence of Water on Plastic Deformation of Olivine Aggregates: 1. Diffusion Creep Regime. J. Geophys. Res. Vol. 105(21), 457-21,469.

Mei, S., Bai, W., Hiraga, T. and Kohlstedt, D.L. (2002), Influence of melt on the creep behaviour of olivine – basalt aggregates under hydrous conditions. Earth Planet. Sci. Lett. Vol. 201, 491 – 507.

Milke, R., Wiedenbeck, M. & Heinrich, W. (2001), Grain boundary diffusion of Si, Mg, and O in enstatite reaction rims: a SIMS study with isotopically doped reactands. Contrib Mineral Petrol, Vol. 14, 15-26.

Mysen B.O. (1983), The structure of silicate melts, Ann. Rev. Earth Planet Sci., Vol. 11, 75-97.

Mysen, B.O. (1988), Structure and Properties of Silicate Melts. Elsevier, pp 354.

Mysen, B.O. (*2003*), Physics and chemistry of silicate glasses and melts. Eur. J. Mineral. Vol. 15, 781-802.

Mungal, J.E. (2002), Empirical models relating viscosity and tracer diffusion in magmatic silicate melts. Geochim. Cosmochim. Acta., Vol. 66 (1), 125-143.

Nascimento, M.L.F. and Zanotto, E.D. (2006), Mechanisms and dynamics of crystal growth, viscous flow and self-diffusion in silica glass. Phys. Rev. B, Vol. 73, 024209.

Nicolas, A. and Ildefonse, B. (1996), Flow mechanism and viscosity in basaltic magma chambers. Geophys. Res. Lett., Vol. 16, 2013-2016.

Ojovan, M.I. and Lee W.E., (2004), Viscosity of network liquids within Doremus approach. J. Appl. Phys. Vol. 95, 3803-3810.

Paterson, M.S., (1982), The determination of hydroxyl by infrared absorption in quartz, silicate glass and similar materials. Bull. Mineral., Vol. 105, 20-29.

Paterson, M.S. (2001), A granular flow theory for the deformation of partially molten rock. Tectonophysics, Vol. 335, 51-61.

Pharr, G.M. and Ashby, M.F. (1983), On creep enhanced by a liquid phase. Acta Metall., Vol. 31, 129-138.

Raj, R. (1982), Creep in polycrystalline aggregates by matter transport through a liquid phase. J. Geophys. Res. Vol. 87, B6, 4731-4739.

Raterron, P., and Jaoul, O. (1991) High-Temperature deformation of diopside single crystal, 1: Mechanical data. J. Geophys. Res., 96: 14,277-14,286.

Raterron, P., Ingrin, J., Jaoul, O., Doukhan, J.C., and Elie, F. (1995) Early partial melting of diopside under high-pressure. Phys. Earth Planet. Int., 89: 77-88.

Rubie D.C. (1986), The catalysis of mineral reactions by water and restrictions on the presence of aqueous fluid during metamorphism. Mineral. Mag., Vol. 50, 399-415.

Russell, J.K. and Giordano, D. (2005), A model for silicate melt viscosity in the System CaMgSi2O6–CaAl2Si2O8–NaAlSi3O8. Geochim. Cosmochim. Acta Vol. 69, 5333-5349.

Reid, J.E., B.T. Poe, D.C. Rubie, N. Zotov, and Wiedenbeck, M. (2001), The self-diffusion of silicon and oxygen in diopside ($CaMgSi_2O_6$) liquid up to 15 GPa. Chem. Geol., Vol. 174, 77–86.

Rybacki, E. and Dresen, G. (2000), Dislocation and diffusion creep of synthetic anorthite aggregates. J. Geophys. Res., Vol. 105 (B11), 26017-26036. DOI:10.1029/2000JB900223

Schäfer, F.N. and Foley, S.F. (2002), The effect of crystal orientation on the wetting behaviour of silicate melts on the surfaces of spinel peridotite minerals. Contrib. Meneral. Petrol., Vol. 143(2), 254-262.

Schiano, P., Clocchiatti, R., Shimizu, N., Maury, R.C., Jochum, K.P., and Hofmann, W., (1995) Hydrous, silica-rich melts in the sub-arc mantle and their relationship with erupted arc lavas. Nature vol 377, pages 595–600

Shannon, R. D. (1976), Revised effective ionic radii and systematic studies of interatomic distances in halides and chalcogenides, Acta Cryst., A32, 751–767.

Shimizu, N. and Kushiro, I. (1984), Diffusivity of oxygen in jadeite and diopside melts at high pressures. Geochim. Cosmochim. Acta., Vol. 48, 1295-1303.

Shimizu, N. and Kushiro, I. (1991) The mobility of Mg, Ca and Si in diopside-jadeite liquids at high pressures. In Physical Chemistry of Magmas, Advances in Physical Geochemistry, (eds. L.L. Perchuk and I. Kushiro), Vol. 9, 192-212, Springer-Verlag.

Samae, V., Cordier, P., Demouchy, S., Bollinger, C., Gasc, J., Koizumi,S., Mussi, A., Schryvers, D. and Idrissi, H. (2021) Stress-induced amorphization triggers deformation in the lithospheric mantle. Nature 591, 82–86 (2021). https://doi.org/10.1038/s41586-021-03238-3

Spiess, R., Dibona, R., Rybacki, E., Wirth, R. and Dresen, G. (2012), Depressurized Cavities within High-strain Shear Zones: their Role in the Segregation and Flow of SiO2-rich Melt in Feldspar-dominated rocks. Journal of Petrology, 53 (9). 1767-1776. doi:10.1093/petrology/egs032

Urbain, G. Bottinga, Y. and Richet, P. (1982), Viscosity of liquid silica, silicates and alumino-silicates. Geochim. Cosmochim. Acta, Vol. 46 (6), 1061–1072.

van der Molen, I. and Paterson, M. S. (1979) Experimental deformation of partially-melted granite. Contributions to Mineralogy and Petrology, 70 (3), 299-318. doi:10.1007/bf00375359

Vigneresse, J.L., Barbey, P. and Cuney, M. (1996), Rheological transitions during partial melting and crystallization with application to felsic magma segregation and transfer. J. Petr., Vol. 37, 1579-1600.

Walte, N.P., P.D. Bons, C.W. Passchier and Koehn, D. (2003), Disequilibrium melt distribution during static recrystallization. Geology, Vol. 31, 1009–1012.

Wanamaker, B.J. and Kohlstedt, D.L. (1991), The effect of melt composition on the wetting angle between silicate melts and olivine. Phys. Chem. Mineral., Vol. 18, 26-36.

Wild, B., Daval, D. Micha, J.-S.; Bourg, I.C.; White, C.E. and Fernandez-Martinez, A. (2019), Physical Properties of Interfacial Layers Developed on Weathered Silicates: A Case Study Based on Labradorite Feldspar. J. Phys. Chem. C 123, 40, 24520–24532, https://doi.org/10.1021/acs.jpcc.9b05491

Wolfenstine, J. and Kohlstedt, D.L. (1994), High-temperature creep and kinetic decomposition of Ni_2SiO_4. Phys. Chem. Mineral., Vol. 21, 234-243.

Wang, Z., Dresen, G. and Wirth, R. (1996), Diffusion creep of fine-grained polycrystalline anorthite at high temperature, Geophysical Research Letters, Vol. 23, 3111-3114.

Wark, D.A., Williams, C.A., Watson, E.B. and Price, J.D. (2003), Reassessment of pore shapes in microstructurally equilibrated rocks, with implications for permeability of the upper mantle. J. Geophys. Res. Vol. 108 (B1), 2050. doi:10.1029/ 2001JB001575

Wendlandt, R.F. (1991), Oxygen diffusion in basalt and andesite melts: experimental results and discussions of chemical versus tracer diffusion. Contrib. Mineral. Petrol. Vol. 108, 463-471.

Wilkinson, D.S. (1998), Creep Mechanisms in Multi-phase Ceramic Materials, Feature Article, J. Amer. Ceram. Soc., Vol. 81, 275-299.

Wirth, R. (1996), Thin amorphous films (1-2 nm) at olivine grain boundaries in mantle xenoliths from San Carlos, Arizona. Contrib. Mineral. Petrol., Vol. 124, 44-54.

Yund, R.A. (1986), Interdiffusion of NaSi-CaAl in Peristerite. Phys. Chem. Minerals, Vol. 13, 11-16.

Yund, R.A. (1997), Rates of grain boundary diffusion through enstatite and forsterite reaction rims. Contrib. Mineral. Petrol., Vol. 126, 224-236.

Yund, R.A. and Farver, J.R. (1999), Si grain boundary diffusion rates in feldspar aggregates. Abstr. EOS, supl. F1077.

Zhang, Y., Huaiwei, N. and Yang, C. (2010) Diffusion Data in Silicate Melts, vol. 72, 311-408, Reviews in Mineralogy & Geochemistry. DOI: 10.2138/rmg.2010.72.8

Appendix A

The viscosities of the wetting melts present in samples pmLab from Dimanov et al. (2000) and in samples SilLab1 and SilLab5 (present work) are calculated based on the model of Giordano et al. (2008). The results are shown in Figure A1, where calculated and experimental viscosities are reported as functions of temperature and the number of non-bridging oxygen per tetrahedron, NBO/T (Mysen, 2004).

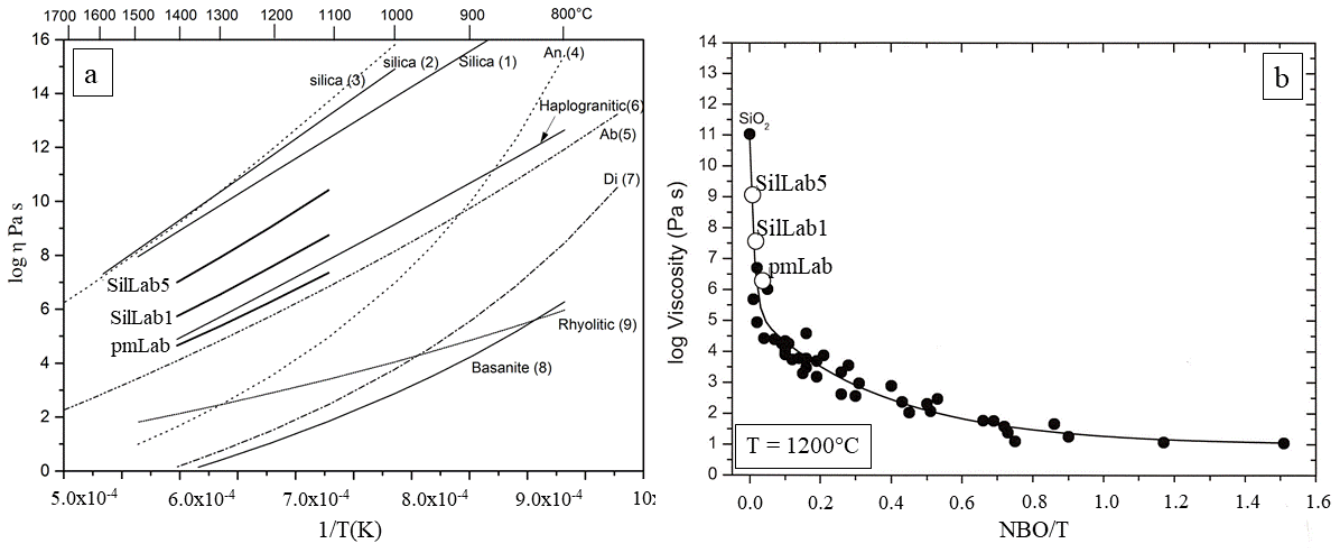

Fig. A1: Comparison between calculated or measured viscosities of typical silicate melts and viscosities calculated for the compositions of the melts present in our materials. a) Arrhenius plot of viscosities of typical silicate melts (not exhaustive, but covering the whole range of viscosities from basaltic composition to vitreous silica) and those of the melts present in our samples (SilLab1 and SilLab5) and in the partially molten samples (pmLab) of Dimanov et al. (2000), computed with the model of Giordano et al. (2008). Data for silica are: (1) from Giordano et al., (2005), (2): from Nascimento and Zanotto, (2006), Silica (3): from Ojovan and Lee (2004) and from experimental data of Urbain et al., 1982 and Hetherington et al (1964). Anorthite (An(4)) and Diopside (Di(7)): from Russel and Giordano (2005), Haplogranitic(6), Albite (Ab(5)) and Rhyolitic(9): from Giordano et al. (2006), Basanite(8): from Giordano et al. (2006). b) Comparison of the experimental viscosities used by Giordano et al. (2008) to set the parameters of their model and the viscosities computed with the latter for compositions of the melts present in our materials as a function of NBO/T (number of non-bridging oxygen per tetrahedron). The solid line is only an eye guiding fit.

Appendix B

The effective molecular diffusion coefficients of the wetting melts present in samples pmLab from Dimanov et al. (2000) and in samples SilLab1 and SilLab5 (present work) are calculated based on the Eyring equation (see text, equation (2)) and the corresponding viscosities shown in Figure A1. The results are shown in Figure B1.

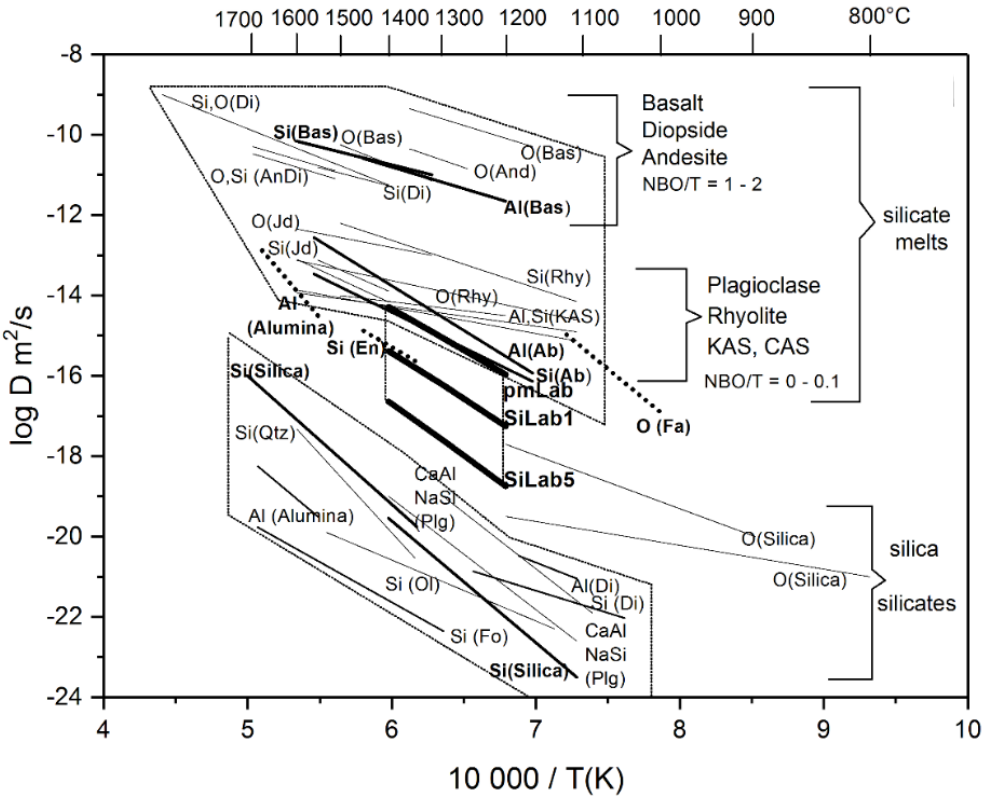

Fig. B1: Arrhenius diagram of volume and grain boundary diffusion of network formers (Si, Al and O) in silicates and oxides and in silicate melts (in dry or unsaturated conditions). The dot line delimited upper and lower fields represent the data for Si, Al and O diffusion in silicate melts and silicate single crystals, respectively. The data are recalculated for a pressure of 0.1 MPa (when activation volumes were available). Bas is basalt, Rhy is rhyolitic melt, Di and Jd refer to diopside and jadeite melts, Ab and KAS are albite and potassium-aluminosilicate melts. Diffusivity of Si in silica falls within the lower field for volume diffusion. Diffusivities of O in silica fall in-between the two fields. Grain boundary diffusivities (recalculated for a grain boundary width of ~ 3 nm) are represented by heavy dot lines. The larger vertical brackets indicate the type of diffusivity. For diffusion in melt the smaller brackets indicate the compositional ranges and the corresponding NBOT numbers. The

diffusivities calculated for our melt compositions (see text) are reported as heavy lines. Diffusion data for melts are from Baker (1990, 1992, 1995), Shimizu and Kushiro (1984, 1991), Canil and Muehlenbach (1990), Wendlandt (1991), Chakraborty et al. (1995), Kress and Ghiorso (1995), Lesher et al. (1996), Harmer and Brook (1980), Brebec et al. (1980), Reid et al. (2001). Data for grain boundary diffusion in silicates, aluminosilicates and alumina are from Rubie (1986), Fisler and Mackwell (1994), Fisler et al. (1997), Fielitz et al. (2004, 2007, 2016). Data for volume diffusion in silicates, aluminosilicates and alumina are from Bejina and Jaoul (1996), Houlier et al. (1990), Jaoul et al. (1981, 1991), Grove et al. (1984), Yund (1986), Le Gall et al. (1994), Fielitz et al. (2007).

Table 2. Mechanical data.

Sample	T (°C)	t (h)	σ_{diff} (MPa)	$d\varepsilon/dt$ (1/s)	d (μm)*
lab-01	1150	31	5.5	7.5×10^{-8}	9.8
	1150	13	10.3	1.3×10^{-7}	-
	1150	8.4	15.3	1.7×10^{-7}	-
	1150	2.4	20.5	2.8×10^{-7}	-
	1150	1.5	30.5	6.4×10^{-7}	-
	1200	0.8	21.3	1.8×10^{-6}	-
	1200	0.5	26.2	3.0×10^{-6}	-
	1200	0.5	31.0	2.8×10^{-6}	-
	1150	25	4.8	8.4×10^{-8}	-
	1150	3.5	20.0	2.7×10^{-7}	9.9
lab-02	1100	17.2	26.2	1.3×10^{-7}	9.8
	1100	23	19.4	8.3×10^{-8}	-
	1100	19.4	22.8	7.8×10^{-8}	-
	1100	15.2	34.1	1.3×10^{-7}	-
	1100	8.4	45.4	2.2×10^{-7}	9.6
lab-03	1100	66	10.1	4.0×10^{-8}	9.8
	1100	21	15.0	5.2×10^{-8}	-
	1100	24.7	19.8	6.9×10^{-8}	-
	1100	24	29.7	8.6×10^{-8}	-
	1100	8.5	39.6	1.2×10^{-7}	-
	1200	4.8	5.2	1.9×10^{-7}	-
	1200	1.6	15.0	6.2×10^{-7}	-
	1200	2.2	10.3	3.9×10^{-7}	-
	1200	1	20.3	1.2×10^{-7}	-
	1200	0.5	25.1	2.1×10^{-7}	-
	1200	0.2	30.0	4.4×10^{-7}	10
lab-04**	1200	72	-	-	9.8

lab-05	1150	20	4.9	$6.0x10^{-8}$	9.8
	1150	24	9.5	$1.1x10^{-7}$	-
	1150	6.5	14.1	$1.7x10^{-7}$	-
	1150	2.0	28.6	$5.0x10^{-7}$	-
	1150	18	6.2	$5.6x10^{-8}$	-
	1150	3.0	23.7	$3.5x10^{-7}$	-
	1150	1.0	38.1	$1.1x10^{-6}$	-
	1225	2.5	5.0	$5.6x10^{-7}$	-
	1225	1.5	9.8	$9.5x10^{-7}$	-
	1225	0.7	14.3	$1.7x10^{-6}$	-
	1225	0.4	19.2	$3.8x10^{-6}$	-
	1225	0.5	13.8	$1.1x10^{-6}$	10
SiLab1-01	1150	21	7.1	$1.4x10^{-7}$	9.3
	1150	3.7	14.2	$3.0x10^{-7}$	-
	1150	3.2	21.3	$4.7x10^{-7}$	-
	1150	1.5	28.6	$8.6x10^{-7}$	-
	1150	15	9.2	$1.5x10^{-7}$	-
	1150	1.8	28.8	$8.3x10^{-7}$	-
	1150	1.8	36.0	$1.4x10^{-6}$	9.2
silab1-02	1200	4	4.0	$1.8x10^{-7}$	9.3
	1200	16	2.7	$1.0x10^{-7}$	-
	1200	2.8	8.7	$3.1x10^{-7}$	-
	1200	1.1	13.5	$5.4x10^{-7}$	-
	1200	1.2	15.02	$5.6x10^{-7}$	-
	1200	1.5	18.2	$7.1x10^{-7}$	-
	1200	1.0	22.9	$1.0x10^{-6}$	9
silab1-03	1100	30	9.7	$2.5x10^{-8}$	9.3
	1100	24.2	14.1	$3.9x10^{-8}$	-
	1100	14	28.4	$5.5x10^{-8}$	-

	1100	11.4	13.5	$7.6x10^{-8}$	-
	1225	2.6	2.7	$4.3x10^{-7}$	-
	1225	1.3	5.7	$6.9x10^{-7}$	-
	1225	0.8	9.1	$1.1x10^{-6}$	-
	1225	1.5	13.8	$1.7x10^{-6}$	-
	1225	1.0	18.6	$2.6x10^{-6}$	9.4
silab1-04	1200	3.1	5.3	$2.8x10^{-7}$	9.3
	1200	1.9	19.5	$6.2x10^{-7}$	-
	1200	1.1	28.8	$1.9x10^{-6}$	-
	1100	12	28.84	$7.4x10^{-8}$	-
	1100	10	43.7	$8.3x10^{-8}$	-
	1150	14.1	5.01	$5.9x10^{-8}$	-
	1150	2.8	19.0	$3.7x10^{-7}$	-
	1150	1.4	24.0	$5.3x10^{-7}$	-
	1225	1.2	5.4	$6.9x10^{-7}$	-
	1225	0.8	14.8	$2.8x10^{-6}$	-
	1225	0.1	28.8	$1.2x10^{-5}$	-
	1225	2.4	4.0	$9.9x10^{-7}$	-
	1225	2.2	5.3	$9.7x10^{-7}$	-
	1225	1.2	10	$2.3x10^{-6}$	-
	1225	0.2	14.5	$6.4x10^{-6}$	9.2
silab5-01	1100	22.4	22.6	$5.3x10^{-9}$	8.6
	1100	28.3	34.1	$1.3x10^{-8}$	-
	1100	36	46.2	$1.5x10^{-8}$	-
	1150	24.2	23.0	$4.8x10^{-8}$	-
	1150	20.5	34.3	$4.3x10^{-8}$	-
	1150	27	47.0	$7.0x10^{-8}$	-
	1200	30.8	5.8	$4.2x10^{-8}$	-
	1200	8.2	16.8	$1.6x10^{-7}$	-

	1200	4.7	22.6	$1.5x10^{-7}$	-
	1200	2.4	33.9	$2.9x10^{-7}$	-
	1200	3.2	45.8	$3.9x10^{-7}$	-
	1200	7.2	34.12	$2.9x10^{-7}$	8.7
silab5-02	1200	23.2	5.00	$5.4x10^{-8}$	8.6
	1200	17.0	9.8	$1.2x10^{-7}$	-
	1200	4.1	19.4	$2.0x10^{-7}$	-
	1200	2.6	29.0	$3.4x10^{-7}$	-
	1200	2.7	38.6	$5.3x10^{-7}$	-
	1200	2.5	43.6	$6.1x10^{-7}$	-
	1225	10.2	5.0	$1.0x10^{-7}$	-
	1225	3.0	9.8	$2.2x10^{-7}$	-
	1225	3.2	19.2	$5.2x10^{-7}$	-
	1225	1.0	28.8	$1.2x10^{-6}$	-
	1225	0.7	38.3	$2.1x10^{-6}$	8.6
silab5-03	1100	163	13.7	$3.6x10^{-9}$	8.6
	1100	125	26.7	$5.3x10^{-9}$	-
	1100	55.8	40.0	$6.9x10^{-9}$	-
	1150	61.6	14.0	$1.8x10^{-8}$	-
	1150	27	27.2	$3.3x10^{-8}$	-
	1150	25	40.3	$5.9x10^{-8}$	-
	1150	20.6	53.8	$5.8x10^{-8}$	8.6
silab5-04	1225	19.2	7.8	$2.2x10^{-7}$	8.6
	1225	4.3	15.0	$4.5x10^{-7}$	-
	1225	2.5	21.8	$7.5x10^{-7}$	-
	1225	1.1	28.8	$1.4x10^{-6}$	-
	1225	0.3	42.9	$3.5x10^{-6}$	8.5
silab5-05	1250	3.0	7.0	$7.1x10^{-7}$	8.6
	1250	1.0	14.0	$1.6x10^{-6}$	-

	1250	0.5	21.0	2.3×10^{-6}	-
	1250	0.2	28.3	5.6×10^{-6}	8.6

* grain size *d* was measured only for the starting material and at the end of each mechanical test.
** lab-04 sample was only annealed in static conditions.